E-Journal of Advanced Maintenance Vol.1 (2009) 1-29
Japan Society of Maintenology

Stress Corrosion Cracking in Low Carbon Stainless Steel Components in BWRs

Shunichi SUZUKI [1,*], Kenrou TAKAMORI[1], Katsuhiko KUMAGAI[1], Akihiro SAKASHITA[2], Norimichi YAMASHITA[2], Chikashi SHITARA[3] and Yuichi OKAMURA[4]

[1] *Materials Engineering Center, Tokyo Electric Power Company (TEPCO), 4-1 Egasaki-cho, Tsurumi-ku, Yokohama 230-8510, Japan*

[2] *Nuclear Asset Management Dept., TEPCO 1-1-3 Uchisaiwai-cho, Chiyoda-ku, Tokyo 101-0001, Japan*

[3] *Nuclear Quality & Safety Management. Dept.,TEPCO 1-1-3 Uchisaiwai-cho, Chiyoda-ku, Tokyo 101-0001, Japan*

[4] *Fukushima-dai2 Nuclear Power Station, TEPCO 12 Kobamasaku, Namikura, Naraha-machi, Futaba-gun, Fukushima 979-0695, Japan*

(Received; January 9th, 2009)

Abstract. In recent years, numbers of SCC have occurred in core shrouds and primary loop recirculation piping made of low carbon stainless steels that had been recognized to be an SCC-resistant material. These incidents resulted in long-term shutdown of Japanese boiling water reactors and have drawn social as well as technical interests.

This paper will provide an introductory review on (1) background of SCC observed in low carbon stainless steel components in BWRs, (2) characteristics of SCC in core shrouds and PLR piping, (3) structural integrity evaluation, (4) SCC mitigation techniques, (5) SCC mechanism and (6) research topics that should be covered regarding these issues.

KEYWORDS: stress corrosion cracking, low carbon stainless steel, L-grade, BWR, core shroud, recirculation piping, PLR, BWR

1. Introduction

In order to ensure safe and stable operation of light water nuclear reactors that supply major part of electric power in Japan, voluntary as well as statutory inspections are being performed periodically. As aging of nuclear reactors progresses, it is becoming commonly recognized that implementing latest technical findings and data to maintenance activities are essential. Based on such consensus, Japanese nuclear regulator (Nuclear and Industry Safety Agency, The Ministry of Economy, Trade and Industry) has issued an evaluation guideline for aging of nuclear power plants. It has deemed that continued safe and stable operation of aging plants can be attained as long as the proper maintenance schedule is followed and revised based on reasonable inspection results using recently-developed techniques and methodologies.

Quantitative understanding of structural material aging as well as lifetime evaluations are important parts of management of aging plants and life extension assessments. Typical aging degradations and failure modes include fatigue, irradiation embrittlement, irradiation-assisted stress corrosion cracking, aging, corrosion, abrasion, etc. Although there still remain arguments on whether stress corrosion cracking (SCC) that usually occurs after certain incubation period should be attributed to aging, it is clearly recognized as the most important phenomenon to be managed to attain safe and stable operation of power plants over a prolonged period.

[*]Shunichi SUZUKI, E-mail: suzuki.shunichi@tepco.co.jp

ISSN – 1883 – 9894/09

In recent years, numbers of SCC incidents have occurred in core shrouds and primary loop recirculation piping (PLR piping) made of low carbon stainless steels that had been recognized to be an SCC-resistant material. These incidents resulted in long-term shutdown of Japanese boiling water reactors (BWRs) and have drawn social as well as technical interests [1].

This paper will provide an introductory review on (1) background of SCC observed in SUS316L components in BWRs, (2) characteristics of SCC in core shrouds and PLR piping, (3) structural integrity evaluation, (4) SCC mitigation techniques, (5) SCC mechanism and (6) research topics that should be covered regarding these issues.

2. Modern History of SCC in Low Carbon Stainless Steels

2.1. Background of Low Carbon Stainless Steel Implementation in BWRs

From the late 1970's, SCC was found in heat-affected zone of SUS304 stainless steel pipe joints of Japanese as well as foreign BWRs [2]. SCC in SUS304 occurs when three primary factors, high tensile stress, corrosive environments and sensitization of the material present simultaneously. From extensive research activities, it was concluded that the root cause of this phenomenon can be attributed to the sensitization; decrease in corrosion resistance at the grain boundary due to the Cr-depletion caused by the chromium carbide precipitation during welding process. For this reason, the applicability of low carbon stainless steels such as SUS304L and SUS316L were evaluated to prevent sensitization. In 1977, SUS316(LC) had been developed by collaborative research project by Japanese BWR owners group. The regulator side (Nuclear Power Engineering Test Center and the Japan Power Plant Institute) had conducted a verification program and concluded that low carbon stainless steels are significantly superior material in SCC resistance and increase the SCC incubation period by 7 to 50 times compared to SUS304 [3].

Based on these evaluations, SUS316(LC) and SUS316L were adopted in PLR piping and in core shrouds in Unit 2 of TEPCO Fukushima dai-2 nuclear power plant (operation started in February 1984) and later units. Simultaneously, a deaeration operation (reducing oxygen level of reactor water) during reactor start up was applied as an environmental mitigation technique and it was then concluded that sufficient treatment methodology was established to prevent SCC from occurring. In the 1990's, however, other incidents were observed in core shrouds of foreign BWR made of SUS304L and of Fukushima dai-2 Unit 3 made of SUS316L

2.2. Early Findings on SCC in Low Carbon Stainless Steels

Considering the SCC in low carbon stainless steel equipment of foreign BWRs, proactive research programs on SCC in low carbon stainless steel were conducted domestically from the mid-1990s. Several characteristics of the SCC in low carbon stainless steels as follows have been revealed through these research programs by the early 2000's.

2.2.1. Findings on SCC initiation

1. Constant load testing

The results of creviced uni-axial constant load SCC test (with a load of $3.5S_m$ (S_m is the maximum allowable stress for the material in the plant design), corrosion potential of 250~280 mV_{SHE}, 620 ºC×24 hours of heat treatment for sensitization), where SCC did not initiate in SUS316L up to 7000 hours, showed that the material was high-resistant to SCC [4]. It should be noted, however, that the surfaces of these test specimens were polished before testing.

2. CBB (Creviced Bent Beam) testing of solution annealed materials [5]

When the surface layer is hardened by heavy grinding and the Vickers hardness exceeds 300HV, SUS316L becomes more susceptible to TGSCC (Trans-Granular Stress Corrosion Cracking) in high temperature water (Fig. 1).

3. Initiation as TGSCC from the machined/ground surface and propagation as ISGSCC (Inter Granular Stress Corrosion Cracking) [6].

CBB tests on SUS316L weld joints with surface machined layer revealed TGSCC initiations and subsequent propagation as IGSCC (Fig. 2). While TGSCC initiation and IGSCC propagation was observed in surface-milled specimens, SCC wasn't found in specimens with no heavy surface machining.

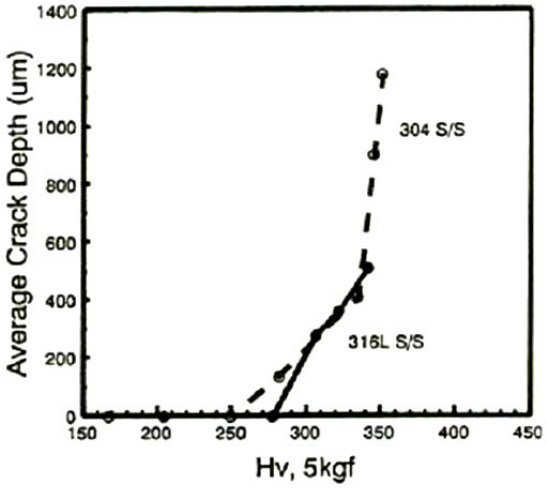

Fig. 1. Relationship between Vickers hardness and the average stress corrosion crack depth in CBB tests

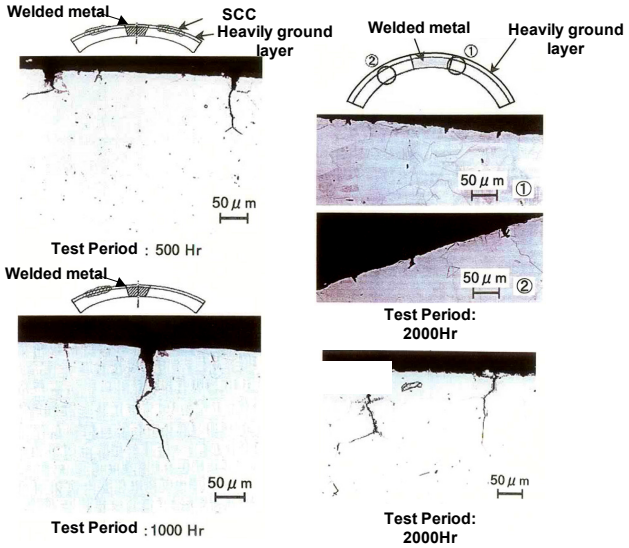

Fig. 2. CBB test results from samples taken from SUS316L welded joints in the Na_2SO_4 injected environment (Dissolved oxygen: 8 ppm, Conductivity: 1.4 μS/cm) at 288ºC,

2.2.2. Findings on SCC growth

The following are findings on the growth rate of SCC of low carbon stainless steels in normal reactor water chemistry and in less aggressive environments such as hydrogen water chemistry.

1. Effects of Corrosion Potential [7]

Figure 3 shows the dependency of SCC growth rate in stainless steels on corrosion potential. All steel types indicated that crack growth slowed with decreasing corrosion potential. Crack growth rate of SUS316L and SUS316NG is lower than that of SUS304 by one order of magnitude. The threshold corrosion potential for SCC growth is -100 mV_{SHE} for low carbon stainless steels, which is higher than that of SUS304 by about 100 mV. The fracture surface showed inter granular crack morphology that looks like "rock candy".

2. Effect of Stress Intensity Factor

SCC growth rate is dependent on stress intensity factor (*K*, hereafter), and drops as the applied *K* decreases. This dependency of SCC growth rates of SUS316L and SUS304 on *K* in normal water chemistry and hydrogen water chemistry are reflected in JSME code, S NA1-2002 [8] (Fig. 4).

2.2.3. Findings on the Effects of Heat Treatment [9]

Even when solution heat treated low carbon stainless steels undergo sensitization heat treatment (e.g. 700 ºC×10 hours), precipitation on grain boundaries or Cr-depletion zone are not formed. However, when the same heat treatment was applied after 10 % cold work, Laves layer precipitation (Fe-Cr-Mo) and W-shaped Cr-depletion layers are observed at grain boundaries (Fig. 5).

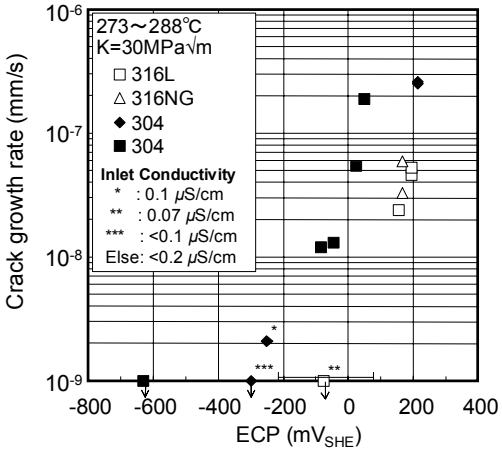

Fig. 3. Effect of corrosion potential on SCC growth rate of austenitic stainless steels

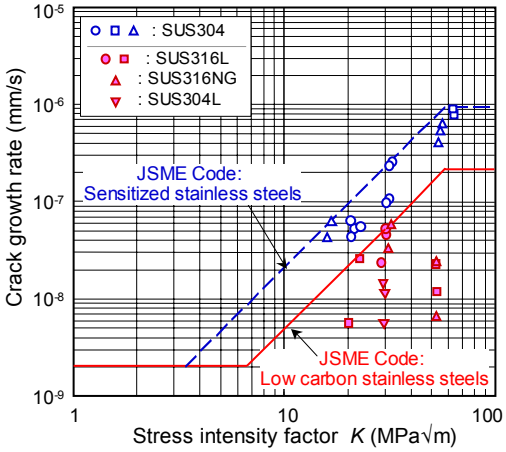

Fig. 4. SCC growth rate disposition curves for austenitic stainless steels in JSME code

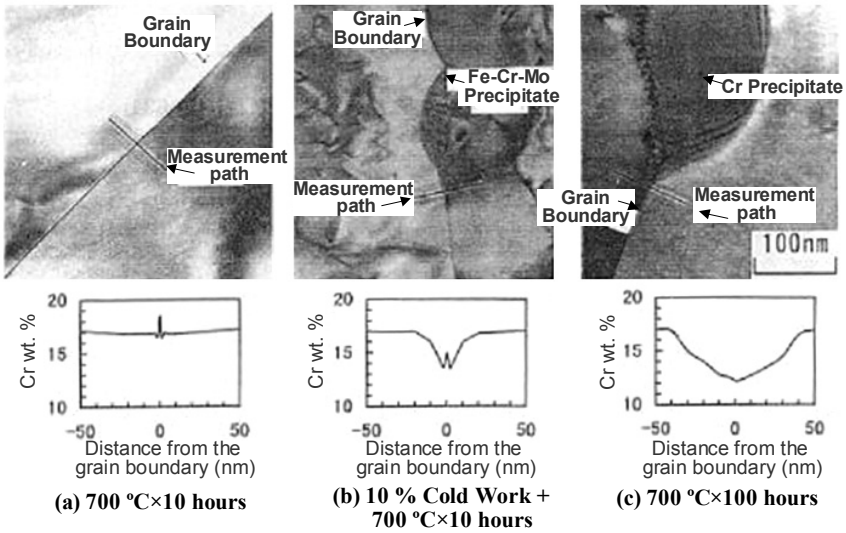

(a) 700 ºC×10 hours **(b) 10 % Cold Work + 700 ºC×10 hours** **(c) 700 ºC×100 hours**

Fig. 5. Effect of heat treatment and cold work on formation of Cr-precipitate and Cr-depletion zone at grain boundaries of low carbon stainless steel

3. SCC in Core Shrouds and Flaw Assessment

Before the implementation of Japanese fitness-for-service standards in July 2001, the first SCC in low-carbon stainless steel component in Japanese BWR was observed in the lower ring weld (H6a) of the core shroud of Fukushima dai-2 Unit 3.

A part of the crack was taken out by EDM (Electrical Discharge Machining) from the shroud material. A detailed examination on the crack was conducted, which revealed the existence of the hardened layer within a range of 300 μm from the surface. The crack morphology in this hardened layer was TGSCC, and that of the subsequent propagation was IGSCC (Fig. 6).

Thorough inspections on low-carbon stainless steel components of all the Japanese BWRs were conducted starting from August 2002 and, as shown in Fig. 7, a number of SCC had been identified [10] by ultrasonic testing (UT) and visual testing (VT). VT on core shrouds were carried out using cameras that have enough resolution to identify a wire with a thickness of 1 mil (1/1000 inch = about 0.025 mm) under water

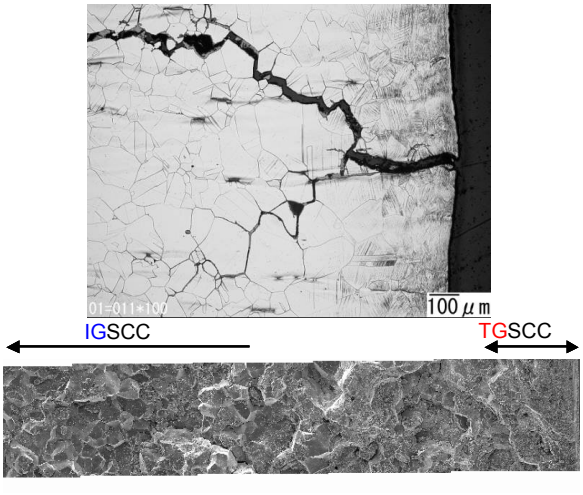

Fig. 6. SCC observed on the edge surface of shroud ring (SUS316L), adjacent to H6 weld of the core shroud of Fukushima dai-2 Unit 3

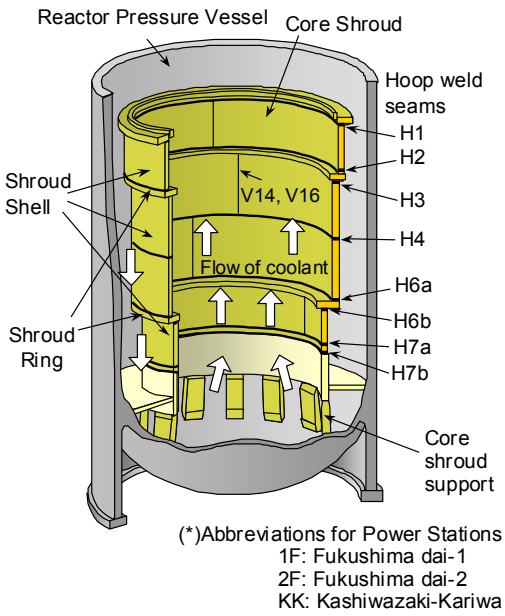

Power Station(*) - Unit	Material	Weld Seam	Face	Location	Number of Crack	Max. Surface Size Width x Height(mm)
1F-4	304L	H4	Inner	Shell	1	180 x 80
2F-2	316L	H3	Inner	Ring	2	30
				Shell	5	30 x 25
			Outer	Weld	3	40 x 17
		H4	Inner	Shell	17	200 x 30
					7	80 x 90
2F-3	316L	H3	Inner	Ring	1	8
					10	210
				Shell	1	13
		H4		Shell/Weld	1	16 x 30
2F-4	316L	H3	Inner	Shell	5	30
		H4			1	31 x 19
			Outer		1	11 x 15
KK-1	316L	H3	Inner	Ring	9	145
		H4	Outer	Shell	1	32 x 22
					3	10 x 20
KK-2	316L	H1	Outer	Ring	1	90
		H6a			Many	–
		V16		Shell	1	20
		H7	Inner	Ring	Many	–
KK-3	316L	H6a	Outer	Ring	Many	–
		H7a	Inner			–
KK-5	316L	H4	Inner	Shell	1	18 x 15
		V14			1	33 x 16

Fig. 7. Schematic showing weld seams in a core shroud and list of observed SCC as of 2002

As shown in Fig. 8, multiple SCC occurred discretely all over shroud ring edges (referred to as “circumferential crack”, hereafter). Due to heavy machining on the surfaces by milling during its manufacturing, a hardened layer of over 300HV was formed as shown in Fig. 9 [11].

In the shroud’s shell, on the other hand, a smaller number of SCC occurred locally along circumferential welds (referred to as “partial crack”, hereafter). The surface crack orientation of these SCC did not necessarily follow the weld line. They seemed to be affected heavily by the multi-axial welding residual stress profile. Some cracks showed a radial propagation on the surface as shown in Fig. 10. A hardened layer of about 50 μm was observed locally at cracked area and was assumed to be formed due to grinder finishing during manufacturing processes. It is assumed that the material hardening in the surface layer enhanced the SCC susceptibility [11].

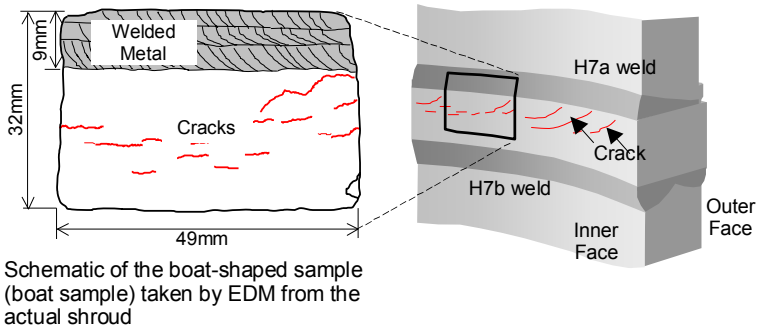

Fig. 8. Schematics showing multiple cracks occurred discretely over the entire circumference of the edge of shroud rings.

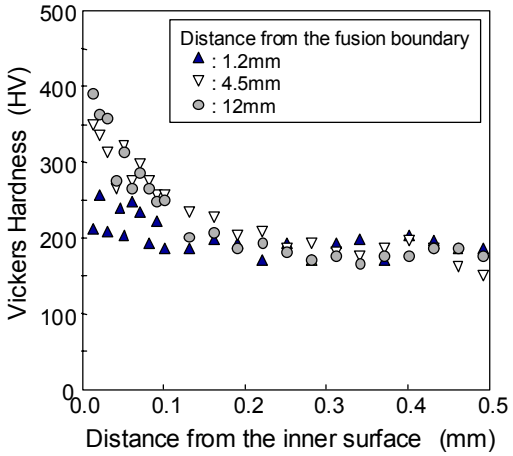

Fig. 9. Vickers hardness profiles in thickness direction measured on the boat-sample taken from the shroud ring (H7a) of Kashiwazaki-Kariwa Unit 3.

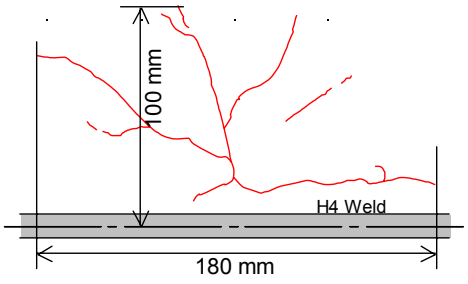

Fig. 10. Example of partial crack observed in the shroud shell, near H4 weld of Fukushima dai-1 Unit 1.

3.1. Fitness-for-Service Evaluations Based on the Code and Standards [10]

3.1.1. Modeling of partial cracks

As shown in Fig. 10, SCC in the shroud shell often showed a two dimensional expansion on the surface, including in axial direction (a direction perpendicular to the weld lines). However, since bending loads become dominant in case of earthquakes, cracks projected to a cross-section perpendicular to the shroud axis have been considered. The projected crack was then modeled as a through-wall crack with the same surface length, and only the circumferential propagation was evaluated, as a more conservative and simplified analysis (Fig. 11).

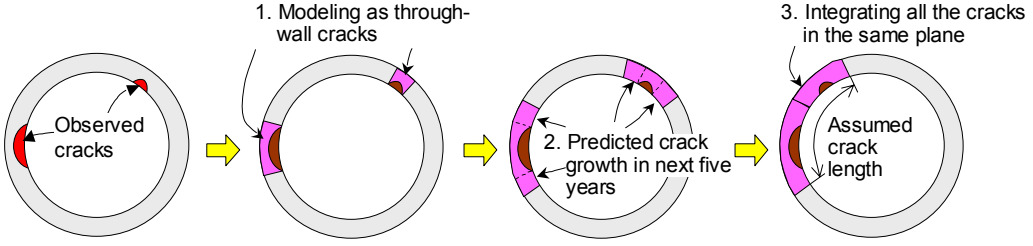

Fig. 11. Modeling of partial cracks in fracture assessments

3.1.2. Modeling of circumferential cracks

Discrete partial cracks that expand over the entire circumference of shroud were modeled as a circumferential crack with a uniform depth as shown in Fig. 12. Average crack depth as measured by UT was used in this modeling.

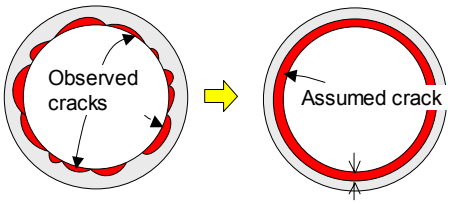

Fig. 12. Modeling of discrete partial cracks expanding over the entire circumference as a circumferential crack in fracture assessments

3.2. SCC Growth Evaluations

3.2.1. Background on SCC growth evaluations

SCC growth analyses are performed referring to the SCC growth rate disposition curve in JSME code. These diagrams are established so that they envelops the maximum value of experimental data obtained from laboratory SCC experiments that simulate actual environmental conditions (Fig. 4).

3.2.2. Crack growth rate for partial cracks

Since the size of partial cracks when they were found was sufficiently smaller than the maximum allowable limit, as will be discussed later, crack growth evaluation of partial cracks was conducted focusing mainly on simplifying the procedure by taking a highly conservative assumption that the crack growth rate is equal to the maximum rate in the JSME disposition curve for low-carbon stainless steel (= 2.1×10^{-7} mm/s) independent of applied K.

In cases in which neutron fluence exceeds 3×10^{24} n/m^2 like weld lines H3 or H4 that are located near the core fuel, the highest rate in JSME disposition curve for sensitized stainless steel (= 9.2×10^{-7} mm/s) was used regardless of the applied K, to take the irradiation effect on SCC growth rate into account.

When multiple cracks were found in the same weld seam, it was assumed that each crack will grow in both circumferential directions at the highest rate. Fracture assessment was then performed by assuming a single crack with a length that is equal to the sum of the predicted length of each crack after 5 years (Fig. 11).

3.2.3. Crack growth rate for circumferential crack

Detailed analyses were performed for circumferential crack growth in the wall-thickness direction considering K vs. crack growth rate dependence, since there is a smaller ligament compared to the cases of partial crack that grows in circumferential direction. Welding residual stress is a dominant factor in SCC growth and is calculated by thermal elasto-plastic finite element (FE) analyses. Prior to an FE analysis, a full-scale mock-up was fabricated using material and welding procedures equivalent to those were used on the actual component. The change in temperature profile with time was measured with thermocouples. Heat input conditions in FE analyses were determined so that the calculated temperature profile will correspond to the actual measurement.

The K-value was calculated using a formula in API-579 [12] since the K formula for a circumferential crack on the outer surface of a cylinder was more appropriate to evaluate cracks in the shroud ring than the formula specified in JSME code as an example assuming a thumbnail crack in a plate.

As examples, welding residual stress distributions for H6a and H7a weld of a shroud of 1100 MW-plant are shown in Fig. 13. The change in K with crack depth and the change in crack depth with time are shown in Figures 14 and 15, respectively. In each figure, (a) shows the result at 12 mm from the H6a fusion line, where cracks had been found in the shroud ring of Kashiwazaki-Kariwa Unit 1; (b) shows the result at 10 mm from H7a, where cracks were found in Kashiwazaki-Kariwa Unit 3.

Since H6a and H7a welds are located at the bottom part of the reactor core, the effect of neutron irradiation is supposed to be insignificant, and the JSME disposition curve for low-carbon stainless steels was referred to in SCC growth evaluations.

In case of the H6a example, there is a large area in the center of the plate where residual stress

becomes compressive and, therefore, *K* becomes 0 at some point during the crack growth, as shown in Fig. 14 (a). For this reason, the evaluation shows that crack will be arrested at about 30 mm from the surface, as shown in Fig. 15.

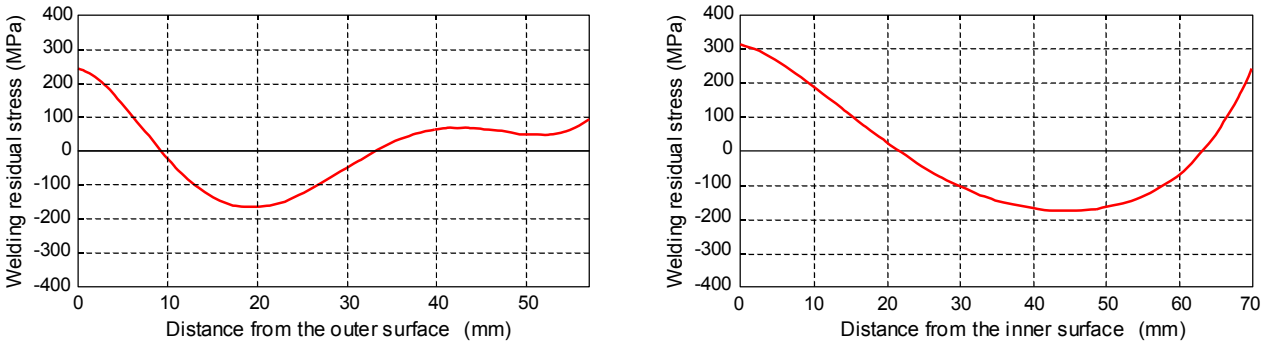

(a) H6a (12mm from the fusion boundary) **(b) H7a (10mm from the fusion boundary)**

Fig. 13. Welding residual stress (axial component σ_z) profiles in plate thickness direction of core shroud rings of a 1100 MW class BWR (by thermal elasto-plastic FEM analyses).

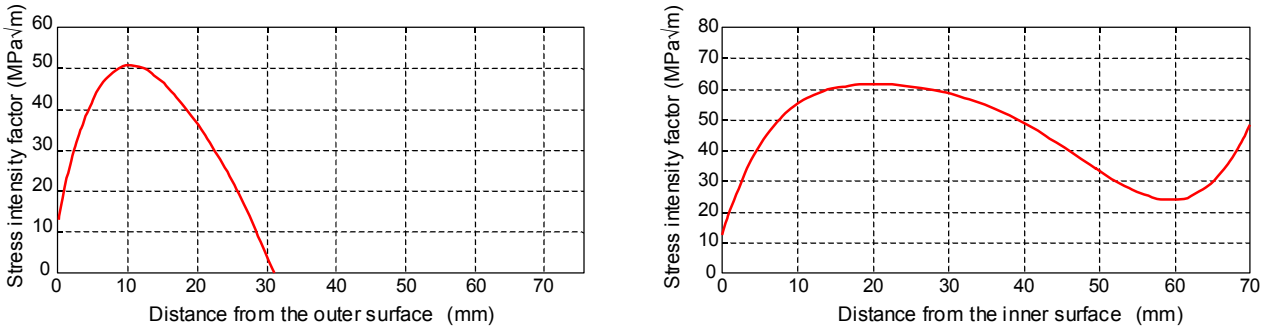

(a) H6a (12mm from the fusion boundary) **(b) H7a (10mm from the fusion boundary)**

Fig. 14. Changes in the stress intensity factor with crack growth for circumferential cracks in H6a and H7a welds of a 1100 MW class BWR (*K*-formulas specified in API579 were used)

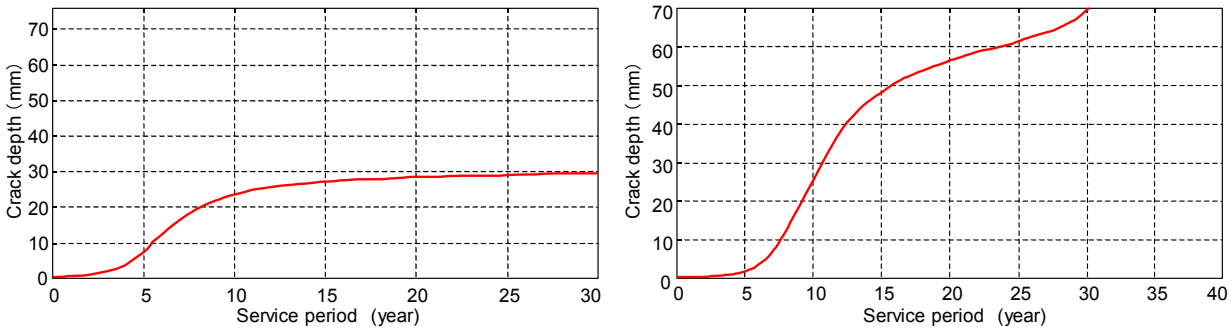

(a) H6a (12mm from the fusion boundary) **(b) H7a (10mm from the fusion boundary)**

Fig. 15. Results of SCC growth evaluations for circumferential cracks in H6a and H7a welds (SCC growth rate disposition curve for low carbon stainless steels in JSME code was used)

3.3. Fracture Assessments [13]

3.3.1. Background on shroud fracture assessments

Primary functions of core shrouds are to support the core fuel and to channel the flow of cooling water within the reactor pressure vessel. Since a shroud is not a part of the pressure boundary and is subjected to relatively low stress during normal operation, it can be regarded that the function and

structural integrity of shrouds are maintained even with some cracks present in them as long as unstable fracture does not occur under the maximum load (= operational load + seismic load) assumed in the shroud design.

3.3.2. Limit load evaluation methods

The plastic collapse is assumed to be the primary fracture mode for components made of highly ductile austenitic stainless steels such as SUS316L and SUS304.

Evaluations are, therefore, performed based on JSME Maintenance Code Attachment E-8; "Limit Load Evaluation Methods" [8]. The most severe loading condition "Operation Conditions I, II + S2" are used, referring to the earthquake response evaluations in the application documents for approval of plant construction. The differential pressure between the inside and outside of the shroud is also considered in accordance to these construction permit application values. Flow stress σ_f is set at 2.7 S_m and the safety factor is set at 1.39 based on the maintenance code.

Considering the maximum load at the time of an earthquake, the maximum allowable crack length L_{lim} was determined so that the stress on the net cross sections of cylinders corresponds to the flow stress.

Figure 16 shows the results of fracture assessments by the limit load evaluation conducted as of 2002 when the cracks were discovered. Figure 16(a) displays the results for partial cracking; the dashed lines indicate the maximum allowable crack length evaluated based on the maintenance codes. As shown in this figure, the structural integrity of shrouds is still maintained even if a half of the entire circumference (about 14~16 m) is separated by SCC. It is also clear from the figure that there still remains enough safety margin even after adding further crack growth assumed in the next 5 year-period.

Results of circumferential crack evaluations shown in Fig. 16(b) indicate that predicted crack length 5 years later does not exceed allowable limits. Considering that the result is drawn based on a conservative modeling of discrete cracks by a circumferential crack, it can be concluded that the integrity of the shroud can be maintained at least during a 5 year-period after the evaluation.

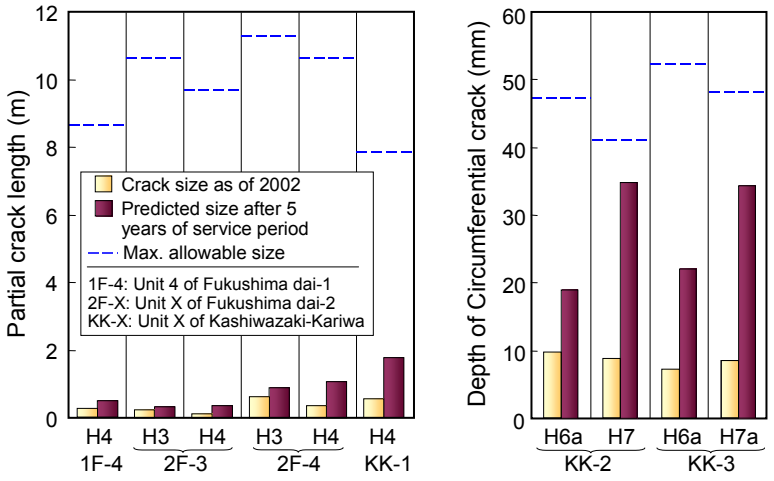

(a) Partial crack **(b) Circumferential crack**

Fig. 16. Results of fracture assessments of core shrouds by limit load analyses.

Since the crack growth rate at H6 weld decreases rapidly as the crack deepens, as shown in Fig. 15, the plant operation leaving the crack present was continued under such conditions that the periodical inspections and structural integrity evaluations based on the code and standard would be conducted.

The latest results of crack sizing as of July 2008 are summarized in Fig. 17 [14-15]. As can be seen in these figures, average crack depths as measured by UT are less than predicted values. From these results, it was confirmed that the current crack growth evaluation procedures provide conservative predictions of crack extension.

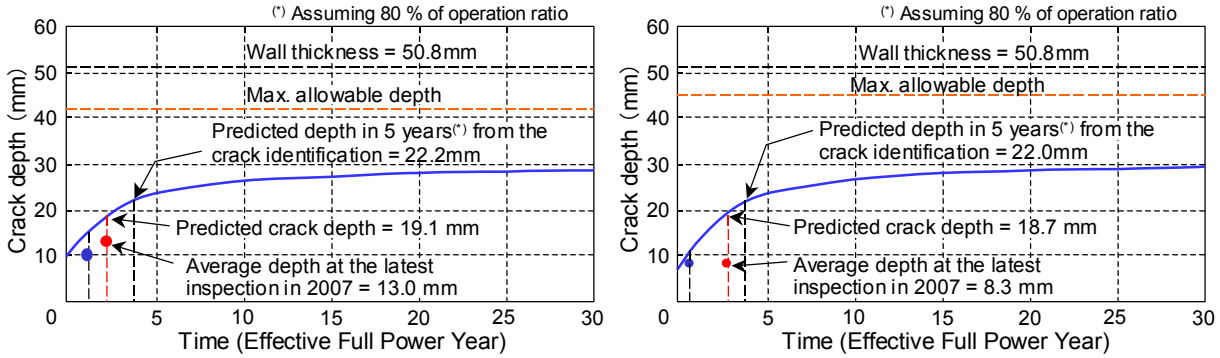

(a) Kashiwazaki-Kariwa Unit 2 **(b) Kashiwazaki-Kariwa Unit 3**

Fig. 17. Change in the average depth of cracks, that are left in H6a weld of core shrouds, during the recent plant operation (Kashiwazaki-Kariwa Units 2 and 3), in comparison with SCC growth predictions using current evaluation code.

3.3.3. Fracture mechanics analysis

The fracture mechanics evaluations were applied to weld joints near the core fuel (H3 and H4) with neutron fluence over 3×10^{24} n/m^2. The K value was calculated for the largest crack found in a weld joint after adding predicted crack extension in the next 5 years to the detected crack size. Fracture assessment was based on the comparison between the evaluated K and the fracture toughness value K_{IC}.

The crack modeling as a through-wall crack as shown in Fig. 11 was also used here. The stress intensity factor was calculated using the K-formula for a through-wall crack along the circumference of a cylinder [16].

$$K = G_m \sigma \sqrt{\pi a}$$

Here,

$\sigma = P_m + P_b$: applied stress
$G_m = 0.2227a(R\cdot t)^{-0.5} + 1$: modification coefficients for curvature
a: half of crack length on the surface

The safety factor (SF) of 1.39 was considered and the maximum allowable crack size was determined as a value that satisfies $K = K_{IC}/SF$. The fracture toughness K_{IC} was assumed to be 165 MPa for locations with the neutron fluence of 3×10^{24}~1×10^{25} n/m^2 and to be 43.2 MPa for locations with 1×10^{25} n/m^2.

Figure 18 shows the results of fracture mechanics evaluations. Fluence of over 1×10^{25} n/m^2 was assumed only in Fukushima dai-1 Unit 4. The allowable crack lengths for Kashiwazaki-Kariwa Unit 1 is smaller because the assumed seismic load in its design was higher than other units. Despite the smaller limit for crack length, the shroud's integrity of all the units was still secured for at least the next 5 years

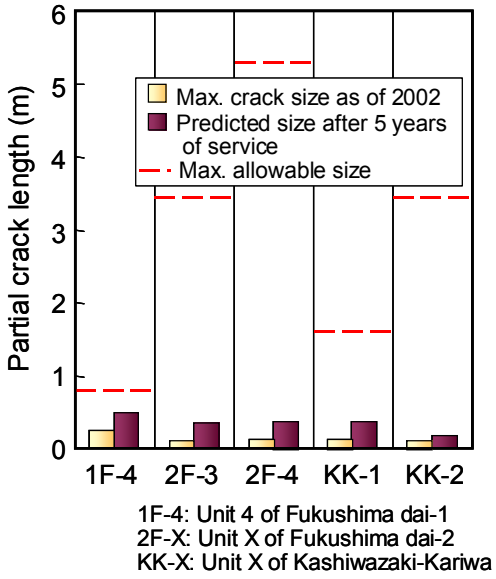

Fig. 18. Results of fracture assessments of H4 welds of core shrouds by fracture mechanics evaluations taking irradiation effects into account.

4. SCC in Recirculation Piping and the Flaw Assessment

Figure 19 shows SCC observed in PLR piping of TEPCO BWRs [17]. A larger number of SCC are found in the main pipe (600A: 600 mm in diameter) compare to smaller pipes with diameters of 300 or 400 mm (300A or 400A, respectively).

So far, SCC were observed only in weld seams with the groove root angle of 30 degrees or larger. Narrow-groove is commonly used in recently-fabricated seams in order to reduce the welding residual stresses and no SCC was found in such seams. The material used for PLR piping is basically low carbon stainless steel SUS316LC (SUS316NG) that is nitrogen-strengthened 316L.

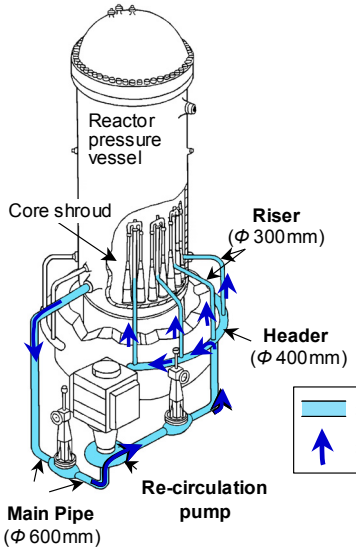

Number of Cracked／Inspected Seams

Diameter of Pipe (mm)		600	400	300	Other
Fukushima -dai2	Unit 1	**1** /6	**0** / 0	**0** /10	**0** / 7
	Unit 2	**4** /43	**0** /16	**0** /22	**2** /33
	Unit 3	**8** /28	**0** /12	**0** /20	**2** /15
	Unit 4	**8** /32	**1** /12	**0** /20	**2** /33
Kashiwasaki -Kariwa	Unit 1	**6** /33	**6** /12	**1** /20	**1** /17
	Unit 2	**4** /29	**0** /12	**0** /20	**0** /16
	Unit 3	**2** /26	**0** /12	**0** /20	**0** /16
	Unit 4	**5** /27	**0** / 8	**0** /20	**1** /19
	Unit 5	**2** /29	**0** /12	**1** /20	**5** /27
Total		**40** /253	**7** /96	**2** /172	**13** /183

Fig. 19. Schematic showing recirculation (PLR) piping and list of observed SCC as of 2002

4.1. Accuracy in Crack Sizing by UT

Before 2002, the accuracy in crack sizing for SCC in SUS304 by conventional UT (using lateral wave and tip echo) had been evaluated by a Japanese national project UTS; “Confirmation Testing for Ultrasonic Inspection Flaw Detectability and Sizing Accuracy” [18]. Based on the evaluations in the program, consideration of assumed error in SCC sizing of 4.4 mm (= as double standard deviation) was required in UT inspections. As shown in Fig. 20(a), however, SCC sizing results [19] showed wider scatter than ±4.4 mm for actual cracks in PLR pipes. One of the main reasons for this larger error is that some cracks have crossed the fusion boundary and have propagated into the weld metal, generating additional echoes reflected from fusion boundaries and kinks in the crack wake that might be judged as tip echoes. Since SCC in SUS304 tends to grow along the Cr-depletion zone in the HAZ rather than propagating into the weld metal, it can be said that this is a specific problem for SCC in low-carbon stainless steels.

However, it was then demonstrated that the comparable level of accuracy can be attained by enhanced UT techniques such as Tip-Echo method using longitudinal wave, Phased Array and so forth, operated by qualified inspectors (Fig. 20(b)) [19].

Based on the consensus that the skill of the inspector has significant effect on the accuracy of UT inspections, the Performance Demonstration System, whose necessity has already been proven in the US, was established recently to provide an objective scale to measure the skill of inspectors.

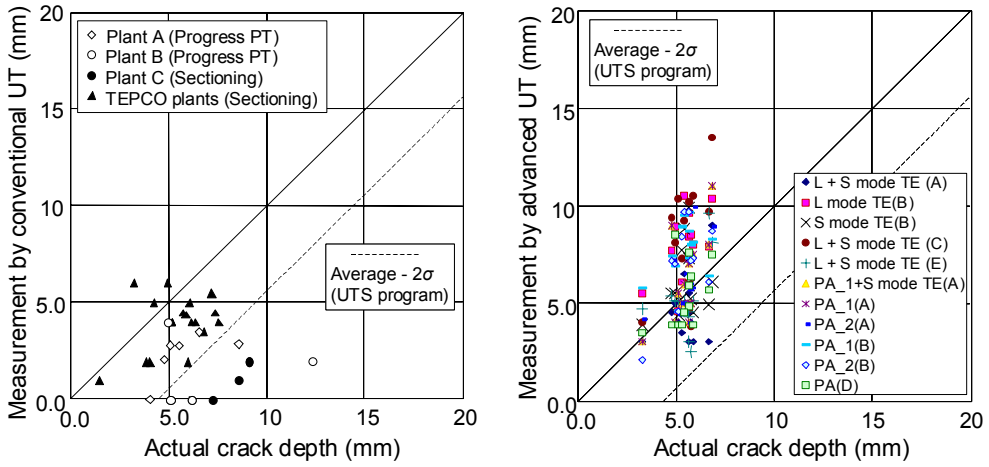

(a) by Conventional UT **(b) by Improved UT**

Fig. 20. Accuracy in the sizing of crack depth (a) by conventional UT technique using lateral wave and (b) by improved UT techniques using phased array, longitudinal wave etc.

4.2. SCC Growth Evaluations

4.2.1. Effect of material hardening on SCC growth rate

Recent research has revealed that the increase in material yield stress due to work hardening etc. can accelerate the SCC growth [20-22]. SCC in a PLR pipe joint propagates in the localized hardened area formed adjacent to the weld root due to thermal deformations during welding, as can be seen in Fig. 21. Since the effect of material hardening on SCC growth rate is not considered in the current JSME disposition curve, there was a concern that evaluations based on the disposition curve can underestimate the possible crack growth.

In order to evaluate the effect of work hardening in PLR pipe joints, SCC growth rate measurements were conducted using CT specimens taken from the weld metal and hardened area in the base material of a full-size mock-up of a PLR joint, as shown in Fig. 22. Results are shown in Fig. 23 with the JSME disposition lines. Although the SCC growth rates of the weld metal shown with solid symbols were enveloped by the disposition curve for low carbon stainless steels, the growth rates of hardened areas shown with open symbols exceeded the curve and it was confirmed that consideration of the hardening effect is necessary for PLR pipe joints.

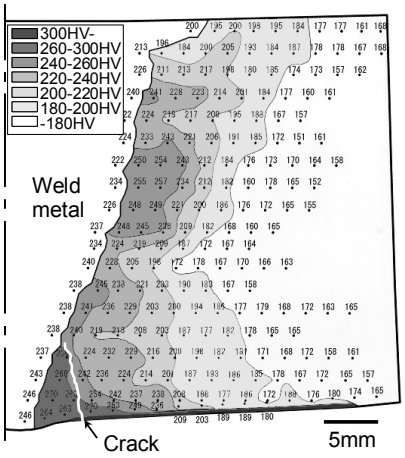

Fig. 21. Vickers hardness profile adjacent to the butt weld-joint of 600A pipe showing hardening adjacent to the root of the weld and in a thin layer on the inner surface.

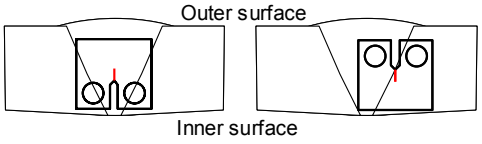

(a) Welded metal **(b) Hardened area in HAZ**

Fig. 22. Schematic showing relative locations and orientations of CT specimens taken from the mock-up of a 600A pipe joint.

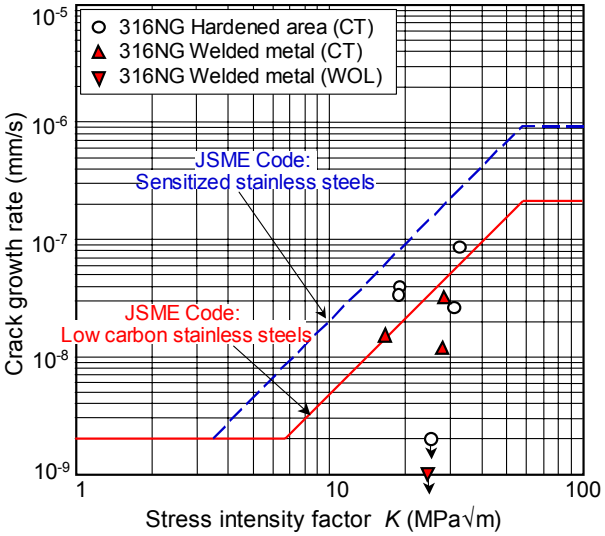

Fig. 23. Crack growth rates obtained from CT samples taken from the weld metal and hardened base metal of the mock-up of PLR joints (600A).

4.2.2. Characteristics of SCC in actual PLR piping [23]

Detailed examinations were performed on cross sections of 77 cracks observed in PLR pipe joints of Japanese BWRs. Figure 24 shows the relationship between the crack depth measured on the cross section and the period of the plant operation. The correlation between the crack depth and the operation period was unclear and very few cracks have propagated more than 10 mm in depth.

Figure 25 shows typical cross sections for SCC in PLR piping. As can be seen in this figure, all the cracks propagated toward the weld metal. The majority of the cracks continue to grow slightly into the weld metal and there are few examples where the crack grew along the fusion boundary as can commonly be seen in case of pipes made of SUS304.

The difference Δd between the crack depth d and critical depth d_c (at which each crack reaches the fusion boundary) was measured on cross sections as shown in Fig. 26 ($\Delta d = d - d_c$). The histogram for Δd (Fig. 27) clearly shows a peak at $\Delta d = 0$, which indicates that many cracks are located near the fusion boundary. Although thorough inspections were conducted within a short time period of 2002 to 2003, and the time when each crack initiated as well as how long they have been propagating varies by cracks, many cracks were identified as their tips just happened to be at the vicinity of the fusion boundary. Therefore, it is reasonable to consider that many of the cracks were arrested or, at least, the crack growth rate remarkably decreased adjacent to the fusion boundaries.

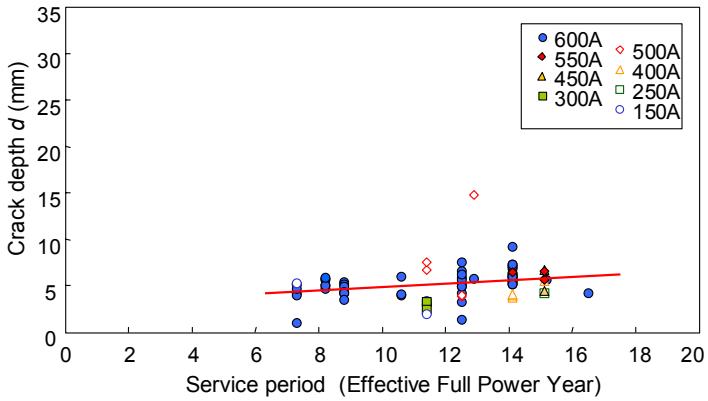

Fig. 24. Relationship between depth of cracks (observed in PLR joints of Japanese BWRs) and operation period of each plant.

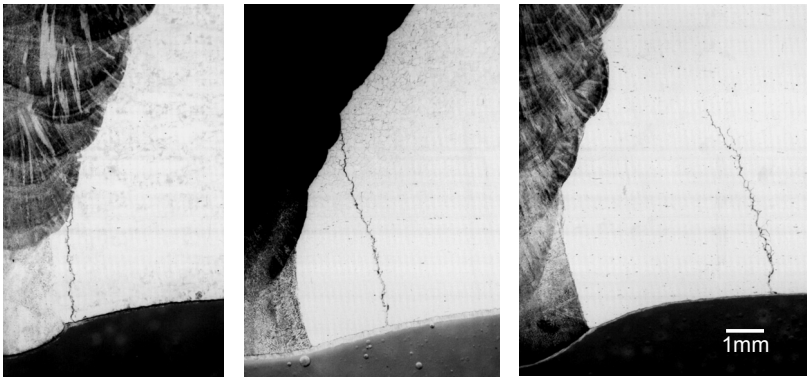

(a) 400A seam **(b) 600A seam** **(b) 600A seam**

Fig. 25. Typical crack morphologies of SCC in PLR weld joints where clear tendency for cracks to grow toward the weld metal was observed.

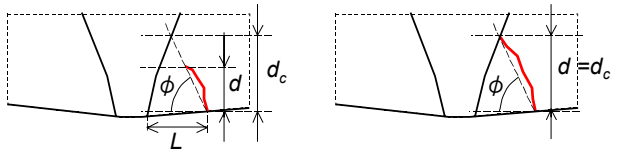

(1) Within the base metal **(2) Arrest at the boundary**

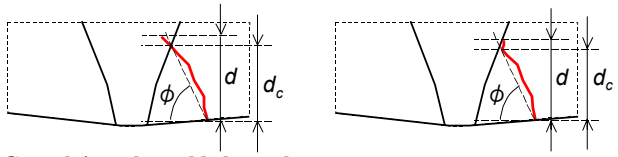

(3) Growth into the welded metal **(4) Growth along the weld interface**

Fig. 26. Classification of SCC morphologies in PLR pipe joints and definition of parameters evaluated.

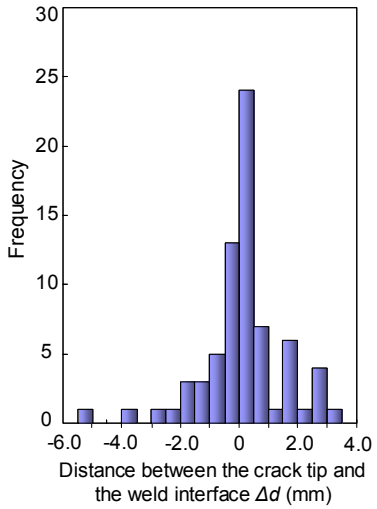

Fig. 27. Frequency of the distance between crack tip and fusion boundary that shows clear peak at near $\Delta d = 0$, which indicates that the tip of many cracks was just on the fusion boundary.

4.2.3. Crack growth evaluation considering the actual crack behavior

Estimated SCC growth behavior in PLR piping based on the examinations on actual components discussed above is schematically shown in Fig. 28. A stress corrosion crack is supposed to: 1) initiate after a certain period of incubation time, 2) grow at a high growth rate in the hardened areas of the base material, 3) arrest or significantly slow down adjacent to the fusion boundary and 4) grow within

the weld metal at a lower rate than that of the hardened base metal.

Although the time periods 1) and 3) have a large impact on the lifetime of actual components, quantitative evaluations are difficult at this moment since both processes include probabilistic uncertainties.

In order to take into account the difference in crack growth rates between periods 2) and 4), the JSME disposition curve for SUS304 in Fig. 23 that envelope the mock-up data was used while the crack is growing within the hardened base metal (depth $d < d_c$). The disposition curve for low-carbon stainless steels was used once the crack was evaluated to be deeper than d_c and to be propagating into the weld metal, since the data from the weld metal of the PLR mock-up were enveloped by this curve.

In Fig. 29, the critical depth d_c, measured on cross sections of actual PLR joints, is shown as a function of L, the distance between the crack initiation site and the fusion boundary. As shown in this figure, a relatively good correlation was observed between d_c and L. As L is measured by UT inspections, the critical depth d_c at which a detected crack reaches the welded materials can be estimated from the relationship shown in Fig. 29.

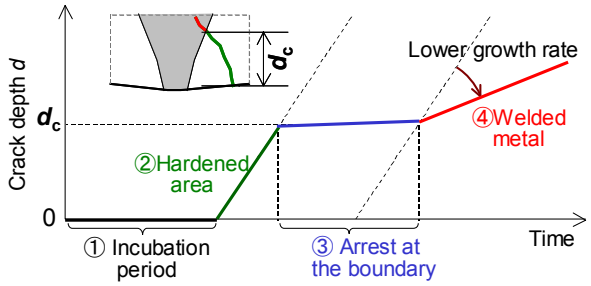

Fig. 28. Crack behavior of SCC in PLR piping suggested by multiple flaw evaluations of actual components.

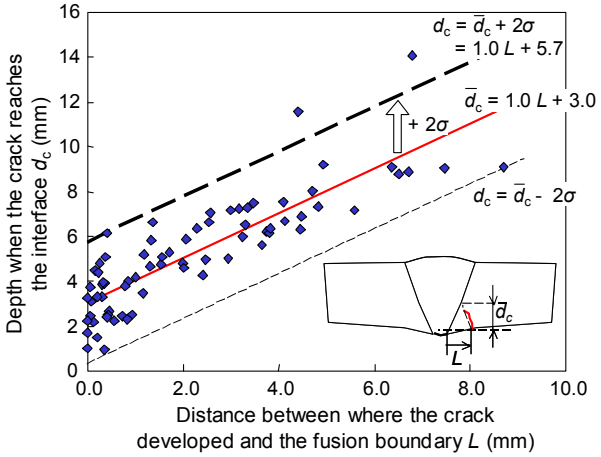

Fig. 29. Relationship between d_c (crack depth when a crack reaches the fusion boundary) and L (distance between the initiation site of the crack and fusion boundary on the inner surface).

4.2.4. Tentative Analysis and Future Problems

Considering the possible error in the measurement of L by UT, the 2σ-offset line of the best-fit line of Fig. 29 is used in the tentative evaluations of the JSME code. Here, σ is the standard deviation assuming the residual follows the normal distribution.

As an example, estimated results for initial cracks with 2 mm depth and 20 mm length located at 4.3 mm from the fusion boundary in 600A (main pipe) and 400A (header) pipes are shown in Fig. 30. In both cases, it was assumed that the crack reaches the interface and growth rate changes at a depth of d_c =10mm. As references, evaluation results, obtained using the disposition curve for SUS304 for the entire period, are shown with dashed lines in Fig. 30.

In the 600A pipe, crack growth rate decreases and the crack slows down rapidly in both cases due to the residual stress profile. In the case of 400A pipe, on the other hand, there is a difference depending on the assumption of the crack growth rate and a significant difference between these calculated results and actual plant data.

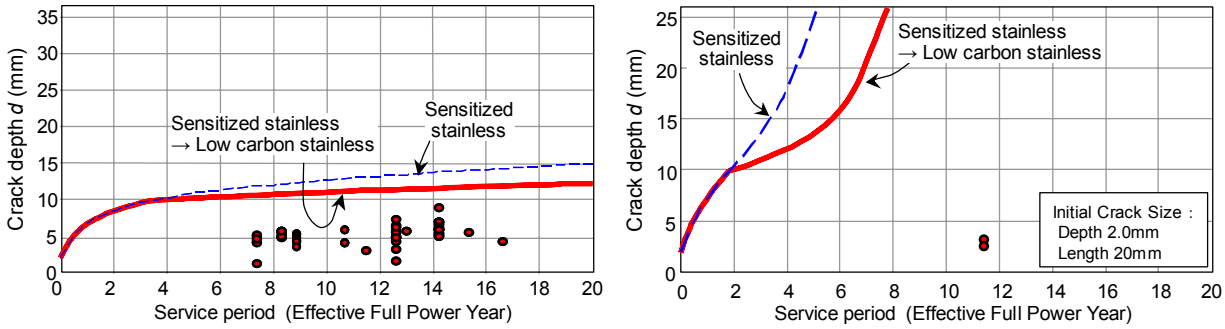

(a) Main Pipe (Φ600 mm) **(b) Header Pipe (Φ400 mm)**

Fig. 30. Examples of SCC growth evaluation using the provisional methodology that uses two different disposition curves, one for hardened base metal and the other for weld metal.

4.3. Examples of the Structural Integrity Assessment Based on Maintenance Codes

Based on the findings described above, structural integrity assessments were performed for 600A and 400A piping. The initial crack size was determined based on the maximum crack size observed in the actual PLR pipes with each diameter (Table 1). The extra margin of 4.4 mm (based on the double standard deviation of sizing error in the UTS project) was added to the initial size, since the PD system for enhanced UT techniques had not been established when the cracks were observed.

According to EB-4420 of JSME code, assessments based on elastic-plastic fracture mechanics were carried out. Detailed procedures of the evaluation are described in Appendix E-9. They are applicable to cracks with their depth less than 75 % of the wall thickness and their surface length less than 1/6 of the circumference. In case of PLR piping, the maximum allowable size is not prescribed by the fracture assessment but by this applicability range of the evaluation procedure.

Table 1 lists the results for the time for a crack to reach the maximum allowable size that was evaluated based on the procedure described in the previous section. The JSME disposition curve for sensitized stainless steel was used for crack growth evaluation within the hardened area.

Table 1 Example of Crack Growth Evaluations and Fracture Assessment of PLR Piping

			600A	400A
Initial Crack Status		Depth (mm)	13.6 (=9.9+4.4)	11.2 (=6.8+4.4)
		Length (mm)	39.0	330
Crack Status when Crack Depth = 75 % of Wall Thickness		Time (year)	> 40	5.2
		Depth (mm)	–	19.5
		Length (mm)	–	223
Crack Status when Crack Length = 1/6 of Circumference		Time (year)	9.8	4.4
		Depth (mm)	14.2	16.5
		Length (mm)	289	190
Evaluation Period (year)			5	4.4
Fracture Assessment at the end of Evaluation Period	Operation Status A, B	Acting Bending Stress (MPa)	4.0	1.7
		Allowable Bending Stress (MPa)	63.0	41.0
	Operation Status C, D	Acting Bending Stress (MPa)	20.4	9.4
		Allowable Bending Stress (MPa)	169	125

For both diameters, the limitation for crack length (<1/6 of the circumference) will first be met after 9.8 and 4.4 years of continued operation in 600A and 400A pipes, respectively. The limitation for crack depth (<75 % of wall thickness) will not be met at least the next 40 years for 600A pipe.

Fracture assessments were performed for the assumed crack size if the plant operation continued for a certain "evaluation period". The evaluation period for 400A pipe was set as 4.4 years from the remnant life before the crack length limitation will be met, whereas 5 years was conservatively used for 600A pipes with remnant life of 9.8 years. Three different criteria for fracture assessment are specified in Appendix E-9, and allowable bending stress was evaluated here as an example. The applied loads considered include internal pressure, thermal loads, own weight, seismic load and welding residual stresses. Welding residual stresses were evaluated using thermal elasto-plastic finite element analysis and other loads were determined using the maximum value assumed in the design of PLR piping with the same diameter among the Japanese BWRs.

As shown in the lower portion of Table 1, acting bending stress at the end of the evaluation period after crack growth was evaluated to be lower than the limit values.

5. Common and Specific Characteristics for SCC in Core Shroud and Recirculation Piping

5.1. Common Characteristics for both Core Shrouds and PLR piping

5.1.1. Existence of the hardened layer on the surface

- Hardened layer over 300HV with a thickness of a few hundred μm was observed on the as-machined surface at the edge of the shroud ring. On the shell of shrouds, hardening was found only at the thin layer on the surface with heavy grinder finishing after welding.
- A thin hardened layer was observed on the inner surfaces of recirculation piping. This surface layer was assumed to be formed during machining to align the bottom faces of the groove. Hardening was also found adjacent to the weld root due to plastic deformation during welding.
- The hardness of the inner surface near the weld root of PLR piping was lower due to annealing by the weld heat input.

5.1.2. Dominant effect of principal stress on the crack orientation

- Surface crack orientation of SCC in low carbon stainless steel was strongly dependent on the principal stress direction, whereas the profile of the sensitized area has a dominant effect on SCC orientation in SUS304.
- Unlike the SCC in SUS304, some cracks in low carbon stainless steels were not parallel to the weld joint due to the effect of the hoop stress in both core shrouds and PLR piping.
- Cracks initiated by residual stress due to grinding propagated in radial or random directions. This is because residual stress by grinding is significantly anisotropic and grinding direction is usually arbitrary.

5.1.3. SCC mode in crack initiation and propagation

- Initial propagation within the surface hardened layer occurred as TGSCC.
- Subsequent propagation occurred as IGSCC.

5.1.4. Non-sensitized material

No significant Cr depletion zone was observed in HAZ of core shrouds and PLR piping.

5.1.5. SCC propagation into the weld metal

In both core shrouds and PLR piping, the ferrite content of the dilution zone where crack propagated into the weld metal was below 5 %, which may have increased the SCC susceptibility of the weld metal.

5.2. Specific aspects for SCC in core shrouds – Effect of Neutron Irradiation

- Noticeable material hardening was observed around H4 and H3 weld joints located at the center

of core shrouds as neutron fluence increases.

- Neutron irradiation promoted the formation of the Cr depletion zone at grain boundaries that was observed in SUS304L core shroud with fluence of 1.3×10^{25} n/m^2 (>1MeV).

6. SCC Mitigation Techniques

There are some SCC mitigation techniques available for core shrouds to reduce surface residual stress such as laser peening [24], water jet peening [25] (Fig. 31) and surface polishing. Applying these techniques after removing cracks by machining can also be effective.

For PLR piping, on the other hand, Corrosion Resistance Cladding (CRC), removal of surface hardened layer, crack removal, and Induction Heating Stress Improvement (IHSI) [26] are applicable. Heat Sink Welding (HSW) and Narrow Groove/Fine Line Welding (FLW) are also effective to reduce welding residual stress.

As for environmental factors, Hydrogen Water Chemistry (HWC) and Noble Metal Chemical Addition (NMCA) have been applied in multiple BWRs. Those techniques reduce the corrosion potential by lowering the concentration of dissolved oxygen and hydrogen peroxide. The relationship between the amount of hydrogen injection and the corrosion potential is shown in Fig. 32 [27].

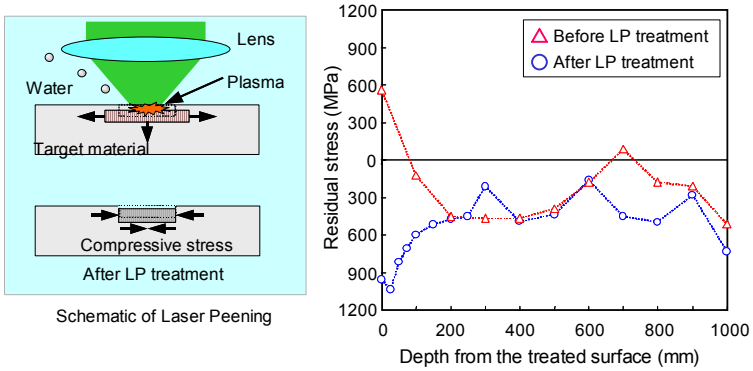

Fig. 31. Schematic of laser peening and its effect in reducing surface residual stress.

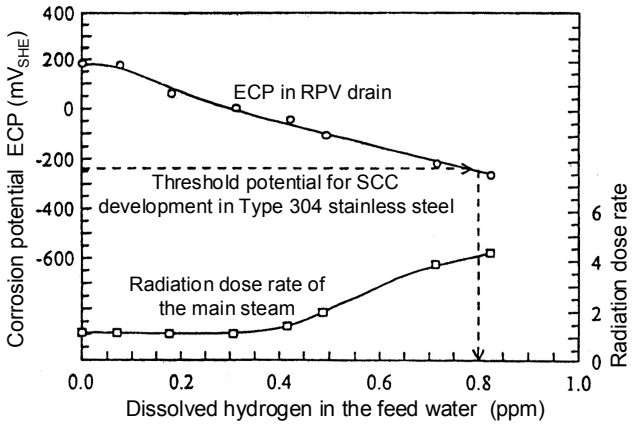

Fig. 32. Effect of dissolved hydrogen in the feed water on the corrosion potential and the radiation dose rate of main steam.

A titanium oxide (TiO_2) injection technique is now being developed [28]. Figures 33 and 34 show the principle of the technique that utilizes Cherenkov light emitted by radiation (gamma-ray)/water interaction within the reactor core. This is a revolutionary technique to prevent corrosion by increasing the anodic current with photo-electric currents.

It is important to select a proper combination of these techniques for each situation.

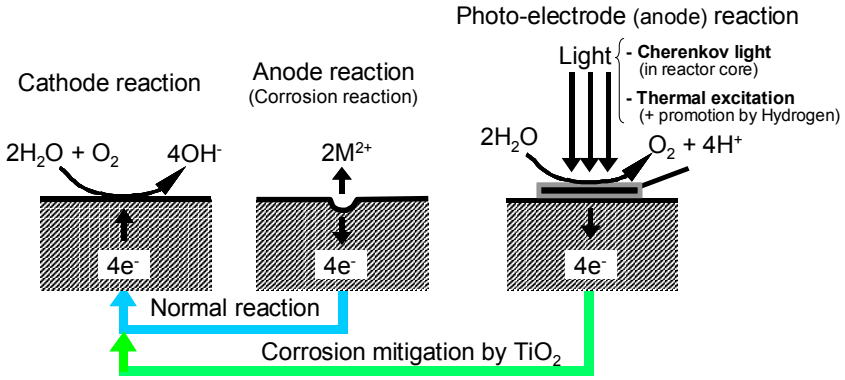

Fig. 33. Principle of SCC mitigation technique by TiO_2 injection.

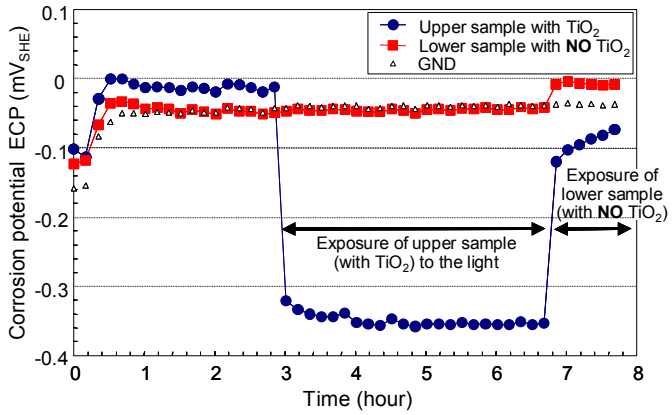

Fig. 34. Effect of TiO_2 injection in lowering corrosion potential.

7. Clarification of the SCC Mechanism

In addition to flaw assessments from the engineering viewpoint discussed above, the mechanistic understanding of SCC on non-sensitized stainless steels is also desirable to ensure the integrity of plant components. A research committee on SCC Mechanism (SCCM committee) had been organized by the Japan Society of Corrosion Engineering. About 60 members are researchers and engineers in fields such as corrosion, welding and metallurgy, from universities, public research institutions, BWR and PWR plant fabricators, metal companies, chemical plant manufacturers and so forth. Research program applications from diversified points of view were submitted by committee members and several programs were selected and funded by the board members of the committee. Accepted research programs focused on root causes for 1) the higher susceptibility of hardened surface layers to SCC initiation, 2) cracks to propagate as IGSCC, and 3) cracking in welded material. Latest results are summarized below.

7.1. Increase in SCC Susceptibility of Surface Hardened Layers

7.1.1. Formation of surface hardened layers [23]

Counter boring prior to welding (machining on inner surface to align grooves) resulted in the extremely thin layer with hardness over 300HV (Fig. 21). Moreover, as can be seen in the example of a main pipe with a diameter of 600 mm in the same figure, the base metal adjacent to the weld root had noticeably been hardened due to heat contraction during welding, and SCC propagated within this hardened area.

7.1.2. Very fine grain layer formed on the surface (Nippon Nuclear Fuel Development, Co., Japan

Atomic Energy Agency, Tohoku University and National Institute for Materials Science)

Fine grain structure layer was found within a depth of several μm from the surface with typical grain size of tens to a few hundred nm [29-31] (Fig. 35, 36).

The oxidation observed in surface fine grain layers suggests that the decrease in corrosion resistance promoted SCC initiation. Similar fine grain layer was also observed on surfaces with heavy machining following weld heat input, which suggests that recrystallization due to the combination of surface machining and heat input is the root cause of the formation of the fine grain layer.

Although a microscopic magnetic layer (martensite phase) was also identified on the surface, it was considered that the layer was not directly related to SCC initiation since the amount of the martensite phase is quite small.

The corrosion resistance of slip bands created by heavy cold work was also found to be low [32] (Fig. 37). In oxygenated high temperature water, generally, a small amount of impurity ions concentrate at the crack tip. Thus corrosivity of the crack tip water chemistry becomes significantly higher than the bulk water, which accelerates the corrosion along slip bands. Considering these findings, SCC is more likely to develop in a trans-granular manner since the number of slip lines is relatively high within the surface layer where the effect of machining is significant.

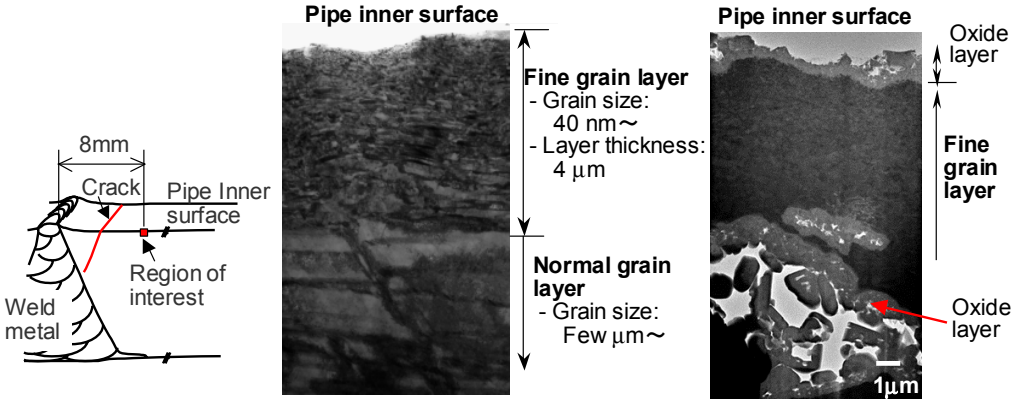

Fig. 35. Very fine grain structure layer observed on the inner surface of the PLR pipe joint.

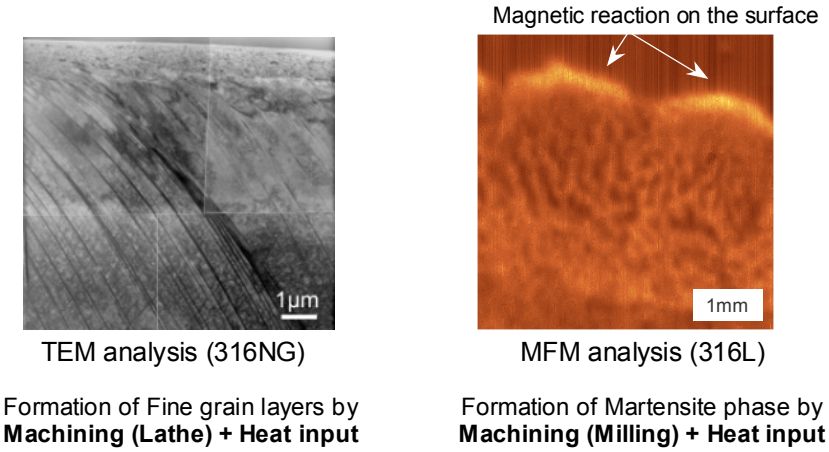

Fig. 36. Fine grain structure formed by combining surface machining and heat input simulating welding.

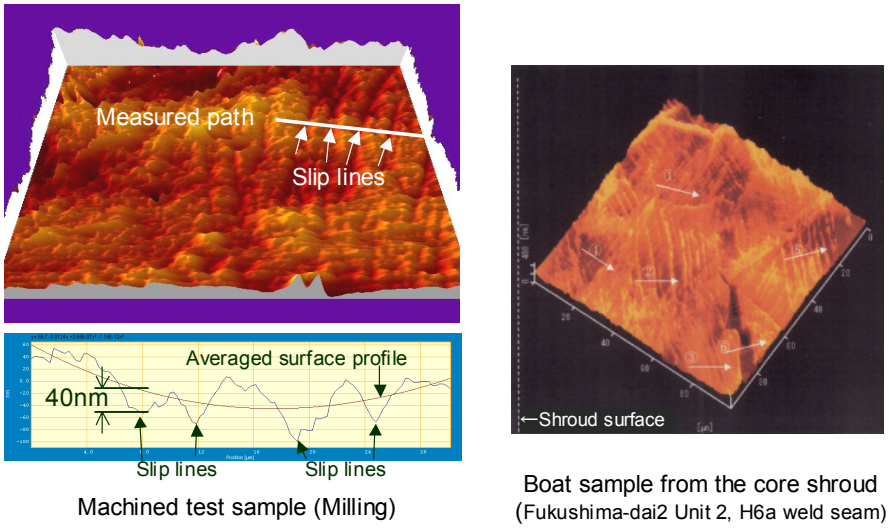

Fig. 37. AFM observation that showed a tendency of preferential corrosion along grain boundaries.

7.1.3. Tensile residual stress formation in surface hardened layers (Osaka University)

Residual stress at the surface can become higher when welding residual stress is added to the original surface stress due to surface machining. Simulation work was conducted on the effect of interaction between surface machining and welding upon the surface residual stress and it was evaluated that approximately 600 MPa of surface residual stress can be generated. (Fig. 38)

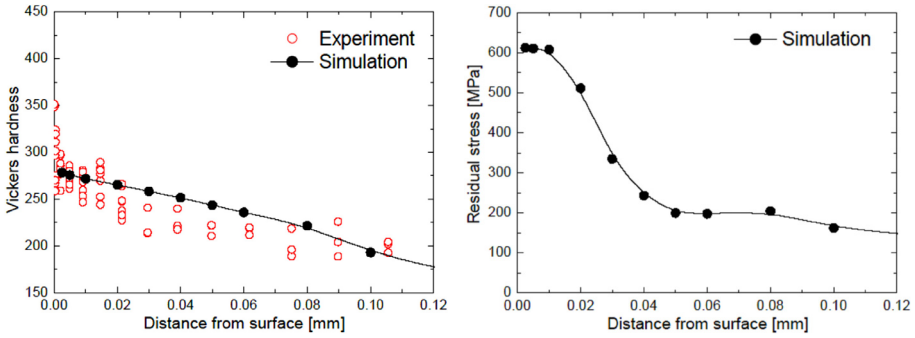

Fig. 38. Results of numerical simulations of the interaction effect between welding and machining on residual stresses.

7.1.4. Threshold stress for TGSCC in surface hardened layers (Sumitomo Metals, Hyogo University and Japan Atomic Energy Agency)

The surface residual stress measurement was conducted in the synchrotron radiation facility Spring-8 in Hyogo, Japan. Four-point bend SCC initiation tests were also performed in a simulated BWR environment. These tests revealed that as it goes deeper inside of the material, the residual stress drops rapidly at a depth of a few to tens of μm and that the threshold surface stress for the TGSCC initiation was 600 MPa [31,33] (Fig. 39). In solution-annealed materials with no surface machining, no SCC was found even at a stress level above the yield stress. These tendencies that surface hardening is necessary for SCC to occur agree well with SCC occurrence observed in actual components.

From discussions above, it can be concluded that current preventive treatments such as surface polishing, IHSI and narrow groove welding for PLR piping as well as surface polishing and peening for core shrouds are effective from mechanistic viewpoints.

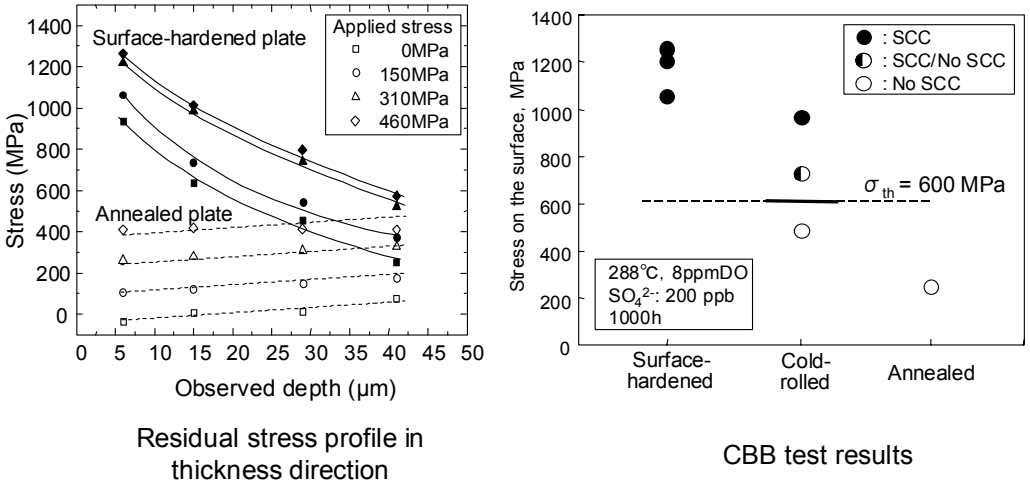

Fig. 39. Comparison between surface residual stress due to machining and tentative threshold stress for SCC initiation obtained from CBB testing.

7.2. Root Cause of IGSCC Growth in Non-sensitized Stainless Steel

7.2.1. Effect of grain boundary deformation on IGSCC growth (Osaka University)

It is important to evaluate the resistance of the grain boundary to slip deformations during loading when evaluating IGSCC growth. Tensile tests on SUS316 with cold work ratios of 0 %, 20 %, 30 %, 40 %, and 60% were conducted at 288 ºC in vacuum at a strain rate of 1.25×10^{-4} /s. Differences in mechanical properties between intra-grain and grain boundary were evaluated as a function of the cold work ratio.

Results showed that the slip at grain boundaries was small below 20 % cold work, but the material was more susceptible to deformations when cold work ratio exceeded 30 %. Vickers hardness values for 20 and 30%-cold work materials are roughly 230 and 300, respectively. As shown in Fig. 40, the change in crack growth rate versus grain boundary slip/hardness and that versus grain boundary slip susceptibility show similar profiles [33]. This suggests that IGSCC growth rate is an increasing function of the susceptibility to grain boundary slip.

Although it remains unclear whether this grain boundary slip triggers SCC or it occurs as a result of SCC, it was at least confirmed that strain concentration occurred as applied load increased. Considering this observation, higher strain energy due to strain accumulation caused oxide film rupture and caused IGSCC growth.

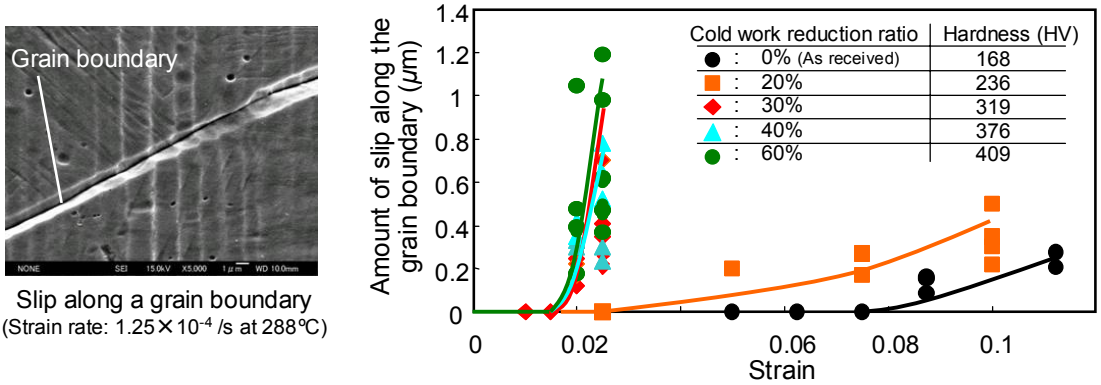

Fig. 40. Relationship between the amount of grain boundary slip and cold work ratio.

7.2.2. Detailed observation on the inside of stress corrosion cracks in actual components

The inside and the tip of stress corrosion cracks taken from actual components were examined by Transmission Electron Microscope (TEM) by PNNL (Pacific Northwest National Lab.) as a TEPCO program. Cr-rich oxide was found at the crack tip and Ni enrichment as well as Cr and Fe depletion was observed in front of crack tips as shown in Fig. 41.

It was supposed from the above observations that the environment at the crack tip was highly corrosive with low corrosion potential and pH, which is quite similar condition that is assumed in SCC in sensitized SUS304. The segregation of Ni, Cr and Fe in front of the crack tip can also imply that the crack was growing at lower rate or even arrested.

From the findings described above, it seemed that similar phenomena were taking place at the tip of SCC in both SUS304 and low carbon stainless steels.

When SCC testing on materials identical to actual components is conducted in an accurately simulated BWR environment, oxide film of a nature identical to that of the actual component is supposed to be observed on crack faces. In typical laboratory testing, however, segregation of alloy elements ahead of the crack tip is less likely to occur, probably due to effects of the deformation taking place adjacent to the crack tip because of the intentionally sustained crack growth. This implies that the crack growth rate results from laboratory tests conservatively evaluate SCC growth behavior in actual plants.

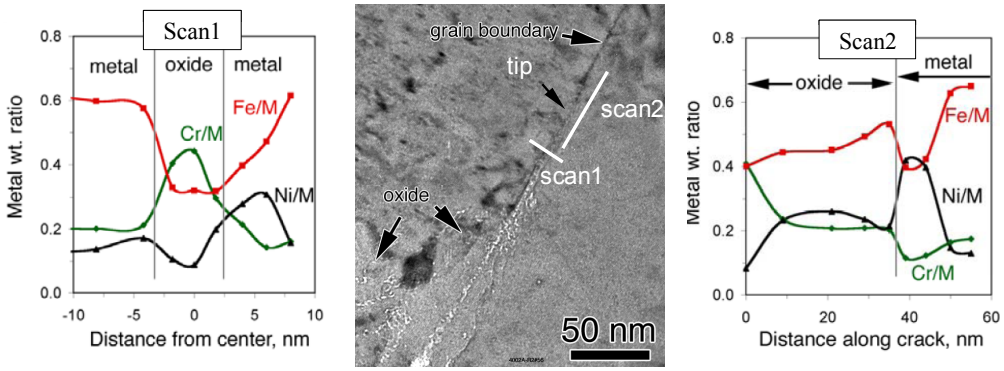

Fig. 41. TEM observation of the inside and the tip of a crack taken from PLR pipe joint of Kashiwazaki-Kariwa Unit 1.

7.3. Summary of SCC Mechanisms

Through the research programs of the SCCM committee, new insights into the mechanism of SCC initiation and propagation were obtained. These new findings are summarized as follows (Fig. 42).

(1) It was experimentally confirmed that surface machining and welding enhances SCC susceptibility. These can be another accelerating factors of SCC initiation and propagation besides sensitization.

(2) Recently performed SCC growth tests seem to be considering SCC promoting factors or crack conditions properly or conservatively, therefore, SCC growth rate disposition curves in JSME code are supposed to be adequate to be applied.

(3) The efficiency of current preventive treatments such as stress reduction, surface polishing and environmental mitigation has also been validated microscopically.

(4) A more quantitative understanding of parameters, such as strain, hardness, threshold stress, grain boundary slip and degradation in corrosion resistance, were identified to be important in this program. Further investigation for other possible factors affecting SCC of low carbon stainless steels mechanistically should be focused in future studies.

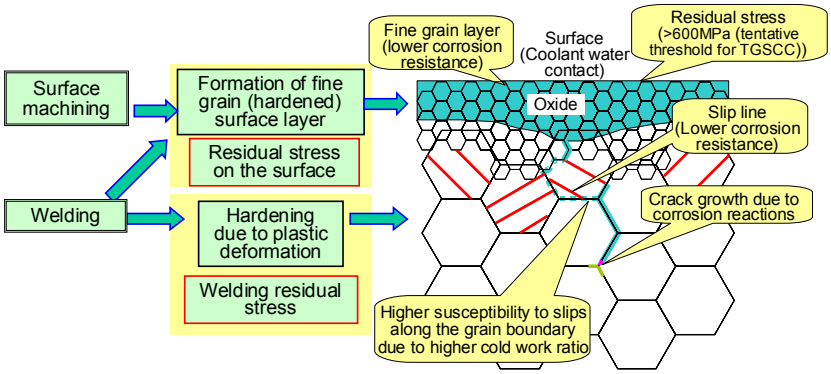

Fig. 42. Summary of the latest findings from research programs focused upon mechanistic understanding of SCC in low carbon stainless steels.

8. The Necessity for Rationalization of the SCC Growth Evaluation Methodology

Due to technical problems remaining in evaluations of SCC such as (1) larger crack sizing error by UT and (2) shortage of data to consider the hardening effect on crack growth rate quantitatively, current evaluation methodology according to the JSME code case requires highly conservative assumptions in each step of the evaluation. As a result, current inspection intervals seems to be unreasonably short considering the actual trend of SCC in core shrouds and PLR piping described in Sections 3 and 4. Establishing more reasonable evaluation methodology based on objective and technical background is, therefore, an urgent task for Japanese BWR owners group.

In order to accumulate data to reduce uncertainties related to the item (2) above, detailed examinations on actual PLR pipe welds removed for replacement were conducted. The summary and future works are as follows.

8.1. Summary of SCC Evaluations on Recirculation Piping

Conservative assumptions required in the current SCC evaluation for PLR piping are:

(1) Possible error in crack sizing by UT: As measured crack depth + 4.4 mm is used as initial crack depth in flow assessments.
(2) Crack modeling: A partial crack is modeled conservatively as a through-wall crack with the same surface length. Discrete cracks over entire circumference are modeled conservatively as a circumferential crack.
(3) Calculation of K: Formula for a crack in a flat plate is used for cracks in a cylinder.
(4) SCC growth rate: Disposition line is drawn so that it envelops all the data ever obtained from laboratory tests.
(5) Crack initiation: A crack is assumed to be present from the beginning of the plant operation neglecting the incubation period for SCC initiation.

Although current crack growth evaluation according to the maintenance code predicts that SCC would grow rapidly and continuously, the majority of the actual cracks are no deeper than 10 mm. Possible reasons for this discrepancy are: (1) many cracks reached and arrested at the weld interface at their depth of around 10 mm, and/or (2) stress intensity factor can decrease as crack grows depending on the residual stress profile, which may result in crack deceleration (negative dK/da effect).

Further rationalization can be attained by taking the incubation period before the SCC initiation or possible crack arrest at the interface into consideration in the crack growth evaluation procedure (Fig. 28).

Applying hydrogen water chemistry as the mitigation technique is beneficial for its effect not only on crack growth rate reduction but also on the extension of the incubation period before SCC initiation. Establishing more reasonable methodology for lifetime evaluation taking such mitigation effects into account properly is desirable (Fig. 43).

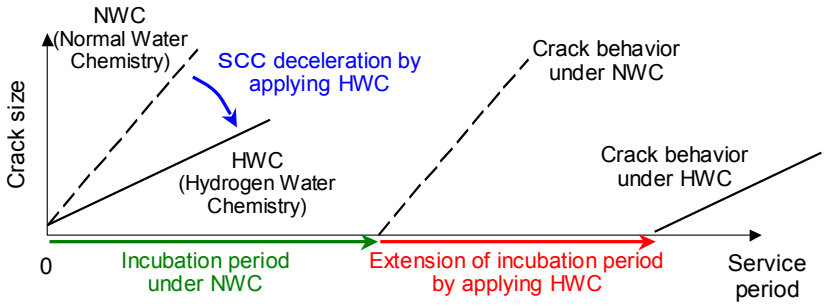

Fig. 43. Consideration of beneficial effects of HWC in SCC growth evaluation.

8.2. Remaining Tasks for Lifetime Evaluation with Higher Accuracy

8.2.1. SCC growth behavior under constant displacement conditions

The change in the stress intensity factor with crack growth differs depending on the welding residual stress profile. Since most of the crack growth rate data are obtained from testing under increasing *K* condition as crack grows, evaluations based on such data can be too conservative when cracks are growing under decreasing *K* condition. And such condition isn't uncommon in actual components depending on residual stress profile (Fig. 44).

FRI model has been developed by Tohoku University to evaluate SCC growth rate based on mechanistic ground [34]. The distinctive feature of this model is that it considers effects of crack tip strain rate on SCC growth rate quantitatively. From this model, it is predicted that crack growth rate drops significantly even at relatively high *K* when *K* decreases as the crack grows. This prediction is consistent with experiment results under constant displacement conditions as well as the actual crack behavior observed in core shrouds (Fig. 45).

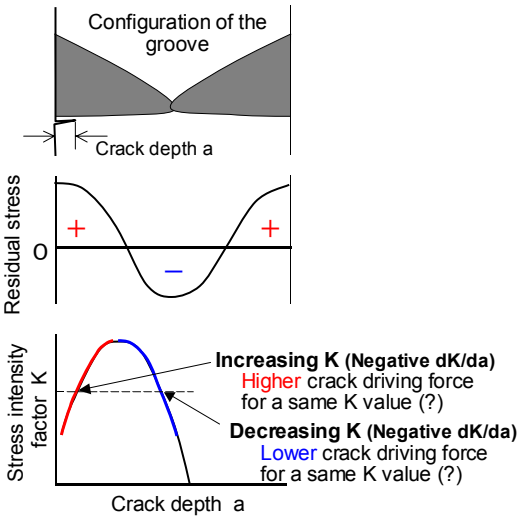

Fig. 44. Effect of residual stress profile on the change in *K* as crack growth and possible effect of differentiation of *K* on SCC growth rate.

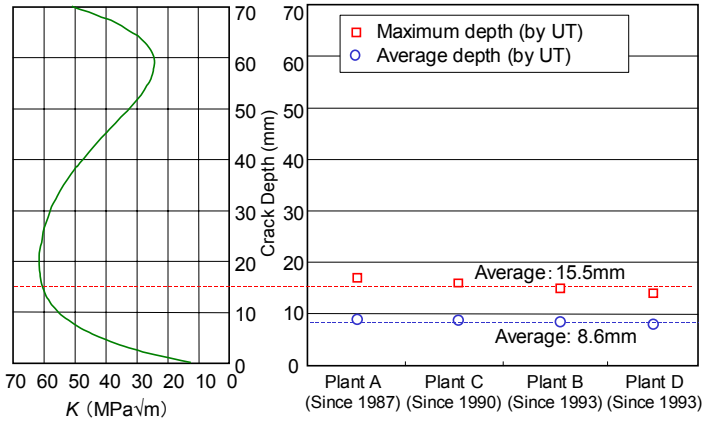

Fig. 45. Change in *K* as a circumferential crack grows at H7 weld of core shrouds in comparison with the average crack depth of SCC observed in H7 welds of 4 Japanese BWRs.

8.2.2. Effect of material hardening on SCC growth rate [35]

Since degree of material hardening adjacent to a crack differs depending on various factors such as pipe diameter, weld condition, crack location, crack path and so forth, applying only one growth rate disposition curve determined with conservative assumptions to all the cracks regardless of the above factors sometimes provides unreasonable prediction of crack behavior.

1. Hardness measurement on actual PLR pipe welds

Quantitative evaluation of hardening effect on SCC growth rate requires (1) the degree of material hardening in the specific weld joint and (2) the quantitative relationship between the degree of hardening and SCC growth rate.

To obtain an insight into the item (1), detailed examinations were performed on 38 PLR pipe weld joints removed from actual BWR plants for replacement. The primary objective was to systematically relate hardness profiles and pipe configurations/weld conditions.

Vickers hardness (HV), yield stress and plastic strain by EBSD (Electron Back-Scatter Diffraction pattern, by GE Global Research as a TEPCO program) measurement were used as measures of the degree of hardening. Small tensile test bars were taken from locations with different HV and tensile tests were performed in air at room temperature.

As can be seen in Fig. 46, yield stress and tensile strength become higher and elongation becomes lower as it goes closer to the root of the weld.

Hardness measurement was also performed at the test section of each specimen. It was confirmed that hardness and yield stress show clear proportional relationship as shown in Fig. 47.

2. Relationship between Plastic Strain and Hardness

Figure 48 shows plastic strain profile near the inner-surface of PLR piping measured by EBSD. Plastic strain is higher near the weld fusion lines and differences between manufacturers are somewhat unclear.

Differences in plastic strain profile by pipe diameters (welded by the same manufacturer) are shown in Fig. 49. This figure indicates that the difference in hardening degree by pipe diameter was significant and that plastic strain increase as pipe diameter increases. From this result, it is understood that the present assessments procedure that uses crack growth rate disposition curve for significantly hardened material regardless the pipe diameter can be excessively conservative for pipes with smaller diameters.

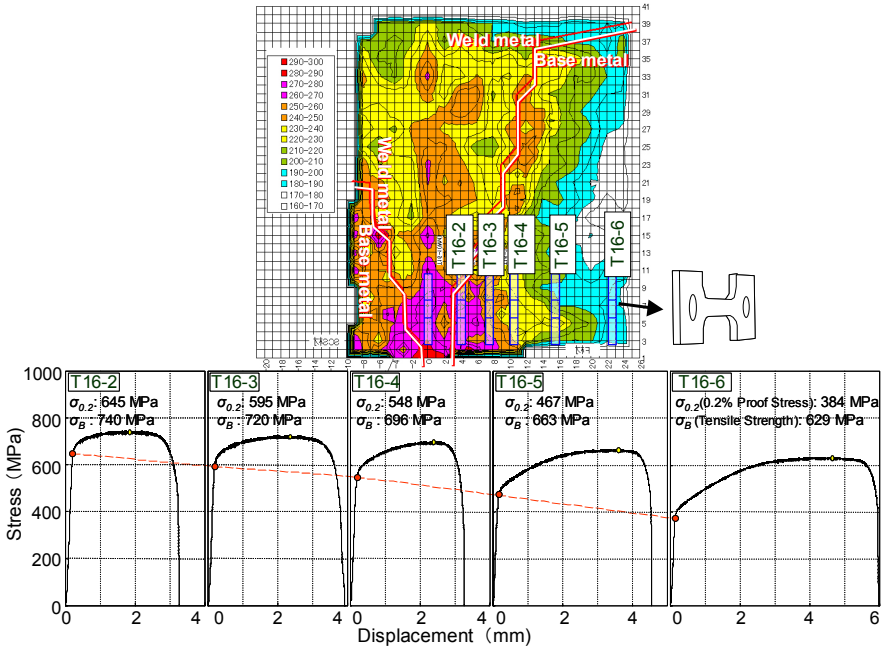

Fig. 46. Difference in tensile properties between locations adjacent to the weld root of a PLR pipe joint removed from Kashiwazaki-Kariwa Unit 1 for replacement.

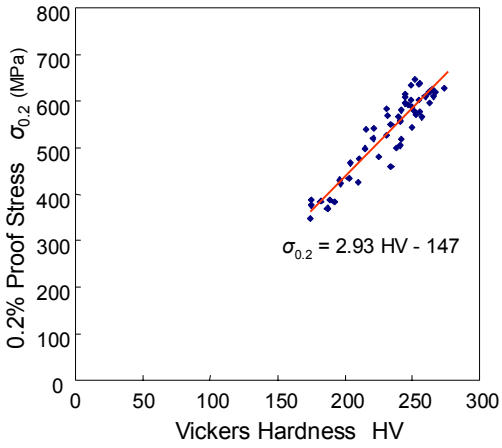

Fig. 47. Relationship between Vickers hardness and 0.2 % proof stress measured on a PLR pipe joints removed from Japanese BWRs for replacement.

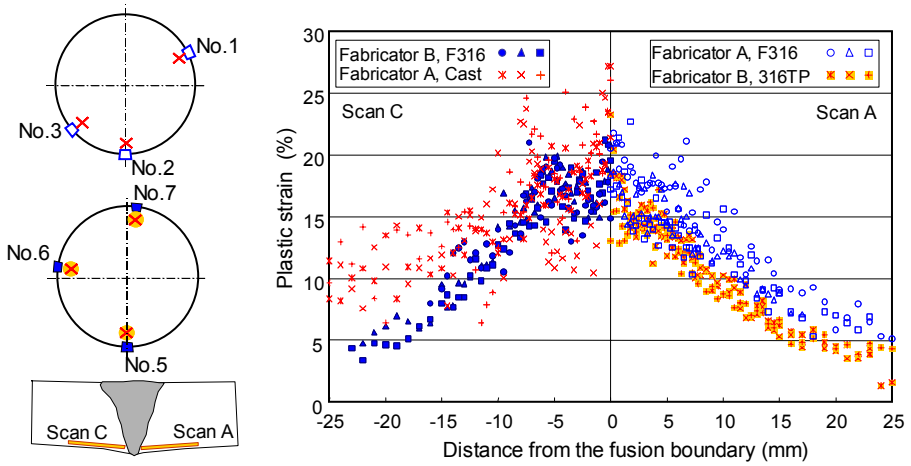

Fig. 48. Difference in plastic strain profiles near PLR pipe joints (600A) between fabricators.

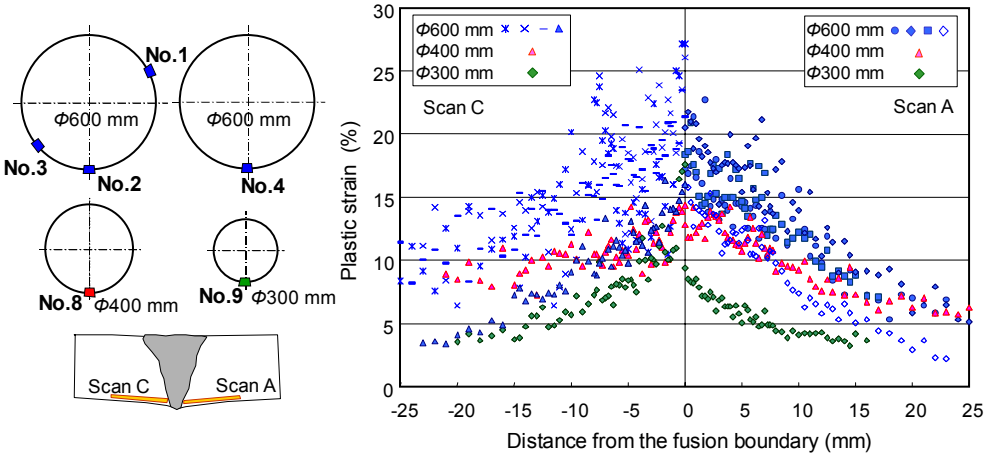

Fig. 49. Difference in plastic strain profiles near PLR pipe joints (Fabricator A) between pipe diameters.

8.2.3. Application of the latest findings to the maintenance code

As discussed above, pipe diameter and crack paths within the hardened area of base metal are not taken into account in the present provisional maintenance code and SCC growth rate for sensitized stainless steel is used in all cases. An extensive SCC growth rate measurement was conducted by JNES (Japan Nuclear Energy Safety Organization) using specimens taken from hardened base metal

and weld metal of full size mock-up of PLR piping [36]. According to their data, the SCC growth rate for sensitized stainless steel is nearly twice as that obtained from a 600A mock-up specimen. Since the degree of hardening of 400A and 300A pipes is even lower, there remains a possibility that the current SCC growth evaluations for medium-diameter pipes become too conservative.

Tentative SCC growth analyses were performed using the SCC disposition curve based on JNES data. The *K* calculation formula for circumferential crack in a cylinder was incorporated in the revised JSME code as of 2004 and was used in these tentative evaluations. Results are summarized in Fig. 50.

Large discrepancies in crack growth behavior were observed, especially in the case of 300A pipe shown in Fig. 50(b) depending on the crack growth disposition curve and *K* formula. As clearly be seen in this figure, current evaluations assuming a crack in flat plates are noticeably conservative.

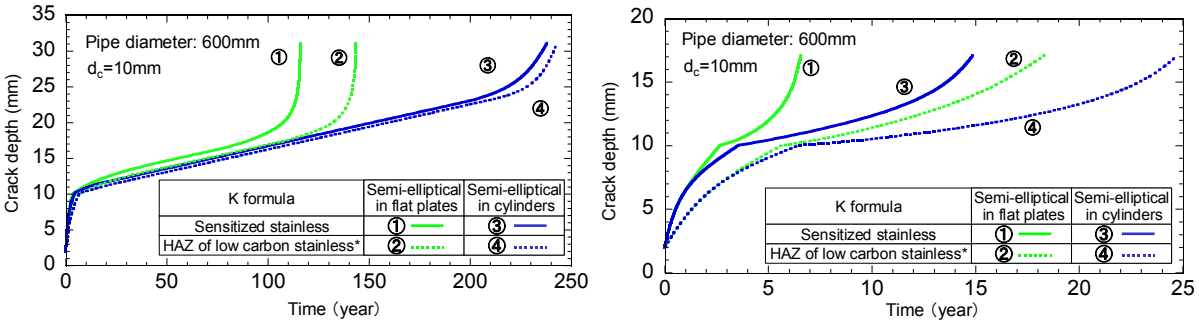

(a) 600A Pipe **(b) 300A Pipe**

Fig. 50. Effect of K-formula and the SCC growth rate disposition curve on SCC growth prediction.

9. Future Topics that Should be Covered

The following is a summary of future tasks to be investigated and data necessary to be accumulated in order to develop more reasonable structural integrity assessment procedure.

(1) SCC growth rate data for cracks within welded metals and HAZ
(2) SCC growth rate data for irradiated material
(3) Threshold stress on the surface with machined layer
(4) Necessary conditions for SCC initiation in weld metals
(5) Further mechanistic understanding on SCC initiation and propagation (materials, stress and environment).

For items (1) to (4), consideration of the effect of water chemistry is also necessary.

Item (1) is especially important to rationalize the structural integrity assessment procedure. Some data will be obtained from research projects conducted by Japanese utilities within the short term, and more extensive testing will be performed through national projects assuming the application of the latest data and findings to the code.

It is expected that the national projects on IASCC will provide valuable data related to the item (2).

Items (3) and (4) will be evaluated through international joint research projects between Japanese utilities and foreign research institutes.

More contributions from universities, national research institutes and specialists in non-nuclear industries are expected, especially in research programs related to item (5). In order to determine a more reasonable interval of inspections of SCC defects, establishing a quantitative procedure for evaluation of the SCC incubation period, considering its probabilistic nature, is desirable.

Increased effort will be made to promote the industry-government-academia research collaboration to obtain high quality and state-of-the-art data and to implement them to the maintenance code and standard promptly after open disclosures.

References

[1] Okamura et al., Trans. of SmiRT 17(2003)
[2] Cheng, C. F., Ellingson, W. A., and Park, J. Y, Corrosion/76, (1976)
[3] Nuclear Power Engineering Test Center, Japan Power Plant Institute; "Present Nuclear Power Facility Reliability Verification Testing" (1984)
[4] Japanese BWR owners group research data
[5] M.Tsubota et al., 7th international symposium on Environmental Degradation of Materials in Nuclear Power Systems - Water Reactors, Vol.1(1995)
[6] TEPCO research data
[7] Ito et al., Proc. 48th Japan Conf. Materials and Environments, JSCE (2001), pp.103-106
[8] JSME, Codes for Nuclear Power Generation Facilities –Rules on Fitness-for-Service for Nuclear Power Plants -, JSME S NA1-2002
[9] Katayama, Proc. 46th Japan Conf. Materials and Environments, JSCE (1999), pp.163-166
[10] Suzuki et al., Maintenology Vol.3, No2 (2004), pp.59-64
[11] Suzuki et al., J. of High Pressure Institute of Japan (JHPI), Vol.42, No4 (2004), pp.13-22
[12] API 579, American Petroleum Institute, "Recommended Practice 579, Fitness for Service"(2000)
[13] Advisory Committee for Natural Resources and Energy, Nuclear and Industrial Safety Subcommittee (4th) Materials
[14] Tokyo Electric Power Company, Press Release, Jul. 10, 2008
[15] Tokyo Electric Power Company, Press Release, Jul. 31, 2008
[16] D.P.Rooke and D.J.Cartwright, "Stress Intensity Factors", Sept.1974
[17] Suzuki et al., Maintenology Vol.3, No.2 (2004), pp.65-70
[18] Japan Power Engineering and Inspection Corporation, Inspection Techniques for Nuclear Power Facilities/Verification Testing for Flaw Detection and Sizing Accuracy of Ultrasonic Testing, 2002 Report
[19] Advisory Committee on Energy and Natural Resources Nuclear Safety and Peace Preservation Subcommittee Nuclear Power Facility Structure Health Evaluation Committee (8th), Japan Power Engineering and Inspection Corporation Confirmation Testing Related to Improving Recirculation Pipe Sizing Accuracy for Ultrasonic Testing
[20] Andresen et al., Corrosion, Paper 02511(2002)
[21] Andresen et al., Proc. 11th international symposium on Environmental Degradation of Materials in Nuclear Power Systems - Water Reactors (2003), pp.816-833
[22] Jenssen et al., Proc. 7th international symposium on Environmental Degradation of Materials in Nuclear Power Systems - Water Reactors (1995), pp.553-562
[23] Kumagai et al., Proc. ASME PVP2004, Vol.479 (2004), pp.217-223
[24] Sano et al., Toshiba Review, 53-10(1998), pp.49-52
[25] Saito et al., J. of Water Jet Technology Society of Japan, 20-1 (2003), pp.4-12
[26] Ishikawajima-Harima engineering review, 18-1 (1978), pp.29-37
[27] Atomic Energy Society of Japan, Reactor Core Chemistry Handbook
[28] Takamori et al., "DEVELOPMENT OF BWR COMPONENTS SCC MITIGATION METHOD BY THE TIO2 TREATING TECHNIQUE", Proc. 13th international symposium on Environmental Degradation of Materials in Nuclear Power Systems - Water Reactors (2007)
[29] Kitsunai and Kodama, Proc. 52nd Japan Conf. Materials and Environments, JSCE (2005), B-212
[30] Ueno et al., Proc. 52nd Japan Conf. Materials and Environments, JSCE (2005), B-210
[31] Takeda et al., Proc. 52nd Japan Conf. Materials and Environments, JSCE (2005), B-205
[32] Nemoto et al., Proc. 52nd Japan Conf. Materials and Environments, JSCE (2005), B-211
[33] Nishimoto et al., Proc. 52nd Japan Conf. Materials and Environments, JSCE (2005), B-207
[34] Shoji et al., 7th international symposium on Environmental Degradation of Materials in Nuclear Power Systems - Water Reactors (1995), pp.881-889
[35] Suzuki et al., Japan Society of Maintenology 2nd Academic Lecture Presentations, 2005
[36] Ando et al., "CGR Behavior of Low carbon Stainless Steel of Hardened Heat Affected Zone in PLR Piping weld Joints", Proc. 13th international symposium on Environmental Degradation of Materials in Nuclear Power Systems - Water Reactors (2007)